Cell Reports

Article

Gαo is a major determinant of cAMP signaling in the pathophysiology of movement disorders

Graphical Abstract

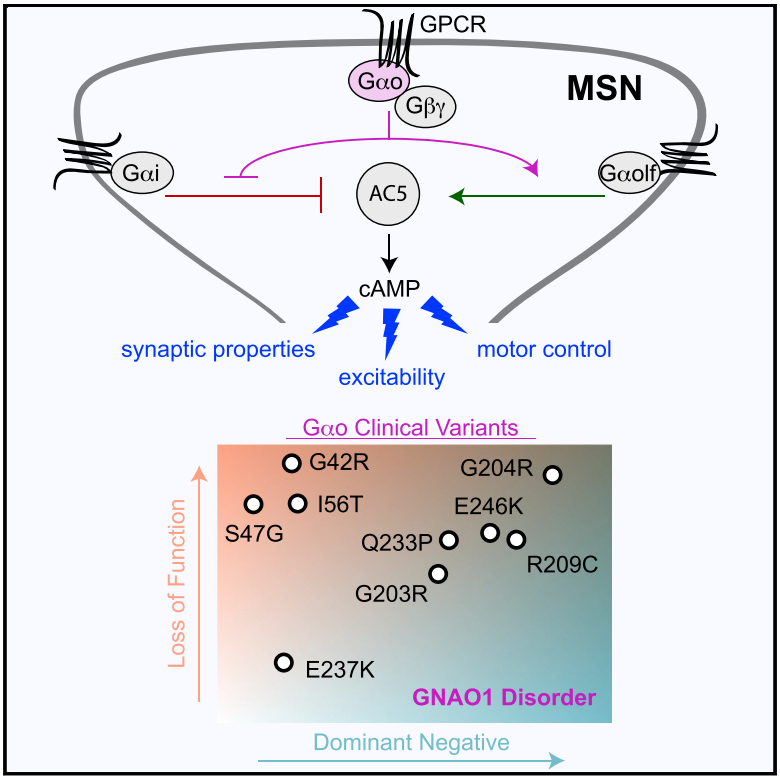

Highlights

- Striatal neurons require Gαo for synaptic function, excitability, and motor control
- Gαo acts to modify both inhibitory and stimulatory GPCR signaling to cAMP
- GNAO1 disease is caused by loss-of-function and dominant-negative mutations in Gαo
- Clinical Gαo mutations produce movement deficits in a circuit-selective fashion

Authors

Brian S. Muntean, Ikuo Masuho, Maria Dao, ..., Randy D. Blakely, Brock Grill, Kirill A. Martemyanov

Correspondence

kirill@scripps.edu

In Brief

Muntean et al. describe biochemical, cellular, and physiological mechanisms by which the heterotrimeric G protein subunit Gαo controls neuromodulatory signaling in the striatum and elucidate mechanisms by which Gαo mutations compromise movements in GNAO1 disorder.

Muntean et al., 2021, Cell Reports *34*, 108718
February 2, 2021
https://doi.org/10.1016/j.celrep.2021.108718

CellPress

Cell Reports

CellPress
OPEN ACCESS

Article

Gαo is a major determinant of cAMP signaling in the pathophysiology of movement disorders

Brian S. Muntean,[1] Ikuo Masuho,[1] Maria Dao,[1] Laurie P. Sutton,[1] Stefano Zucca,[1] Hideki Iwamoto,[2] Dipak N. Patil,[1] Dandan Wang,[3] Lutz Birnbaumer,[4,5] Randy D. Blakely,[2] Brock Grill,[1,3,6] and Kirill A. Martemyanov[1,7,*]

[1]Department of Neuroscience, The Scripps Research Institute, Jupiter, FL 33458, USA
[2]Department of Biomedical Science and Brain Institute, Charles E. Schmidt College of Medicine, Florida Atlantic University, Jupiter, FL 33458, USA
[3]Center for Integrative Brain Research, Seattle Children's Research Institute, Seattle, WA 98101, USA
[4]Neurobiology Laboratory, National Institute of Environmental Health Sciences, Durham, NC 27709, USA
[5]Institute of Biomedical Research (BIOMED), Catholic University of Argentina, Buenos Aires C1107AAZ, Argentina
[6]Department of Pediatrics, University of Washington, Seattle, WA 98101, USA
[7]Lead contact
*Correspondence: kirill@scripps.edu
https://doi.org/10.1016/j.celrep.2021.108718

SUMMARY

The G protein alpha subunit o (Gαo) is one of the most abundant proteins in the nervous system, and pathogenic mutations in its gene (*GNAO1*) cause movement disorder. However, the function of Gαo is ill defined mechanistically. Here, we show that Gαo dictates neuromodulatory responsiveness of striatal neurons and is required for movement control. Using *in vivo* optical sensors and enzymatic assays, we determine that Gαo provides a separate transduction channel that modulates coupling of both inhibitory and stimulatory dopamine receptors to the cyclic AMP (cAMP)-generating enzyme adenylyl cyclase. Through a combination of cell-based assays and rodent models, we demonstrate that *GNAO1*-associated mutations alter Gαo function in a neuron-type-specific fashion via a combination of a dominant-negative and loss-of-function mechanisms. Overall, our findings suggest that Gαo and its pathological variants function in specific circuits to regulate neuromodulatory signals essential for executing motor programs.

INTRODUCTION

G protein-coupled receptors (GPCRs) mediate communication between neurons to regulate complex behaviors (Betke et al., 2012; Bjarnadóttir et al., 2006; Pierce et al., 2002). All GPCRs transduce their signals by activating heterotrimeric G proteins, thereby promoting GTP binding to a Gα subunit and concomitant release of Gβγ subunits (Gilman, 1987; Pierce et al., 2002). Dissociated Gα and Gβγ engage effector molecules to propagate signals. Mammalian genomes encode 16 different Gα subunits with unique signaling properties and influence on effectors (Wettschureck and Offermanns, 2005). Elucidation of the functional roles played by individual Gα subunits *in vivo* is among the most significant challenges in understanding GPCR signaling mechanisms.

One of the most mysterious and intensely studied Gα proteins is G protein alpha subunit o (Gαo), for which a number of mechanisms (Purvanov et al., 2010; Solis et al., 2017) and effectors (Campbell et al., 1993; Ewald et al., 1989; VanDongen et al., 1988) have been proposed. Gαo is one of the most abundant proteins in the brain, highly conserved in evolution and critical for nervous system function (Solis et al., 2017; Sternweis and Robishaw, 1984; Strittmatter et al., 1990; Wolfgang et al., 1990). A particularly controversial subject is the role of Gαo in regulation of cyclic AMP (cAMP), a ubiquitous second messenger regulated by a number of GPCRs. cAMP is critical for many fundamental neuronal processes, including neuromodulation, synaptic plasticity, and excitability (Håkansson et al., 2004; Kandel, 2012). Early *in vitro* studies showed that Gαo does not directly modulate the activity of the cAMP-producing enzyme adenylyl cyclase (AC) (Wong et al., 1992), with the exception of modest effects on the AC1 isoform (Taussig et al., 1994). Nonetheless, in cellular systems, Gαo impacts cAMP production (Feng et al., 2017; Ghahremani et al., 1999). How this occurs remains unclear, primarily due to a lack of tools to disentangle influences of multiple G protein species concurrently activated by GPCRs in an endogenous setting (Sadana and Dessauer, 2009; Sunahara et al., 1996).

Interest in Gαo has been spurred by the discovery that mutations in its gene, *GNAO1*, cause neurological disorders (early infantile epileptic encephalopathy [Online Mendelian Inheritance in Man (OMIM): 615473] and neurodevelopmental disorder with involuntary movements [OMIM: 617493]), collectively referred as GNAO1 encephalopathy (Ananth et al., 2016; Nakamura et al., 2013). Clinical features of this disease include delayed psychomotor development, intractable seizures, and hyperkinetic involuntary movements. To date, 26 unique pathogenic variants in Gαo have been reported (Kelly et al., 2019; Mihalek et al.,

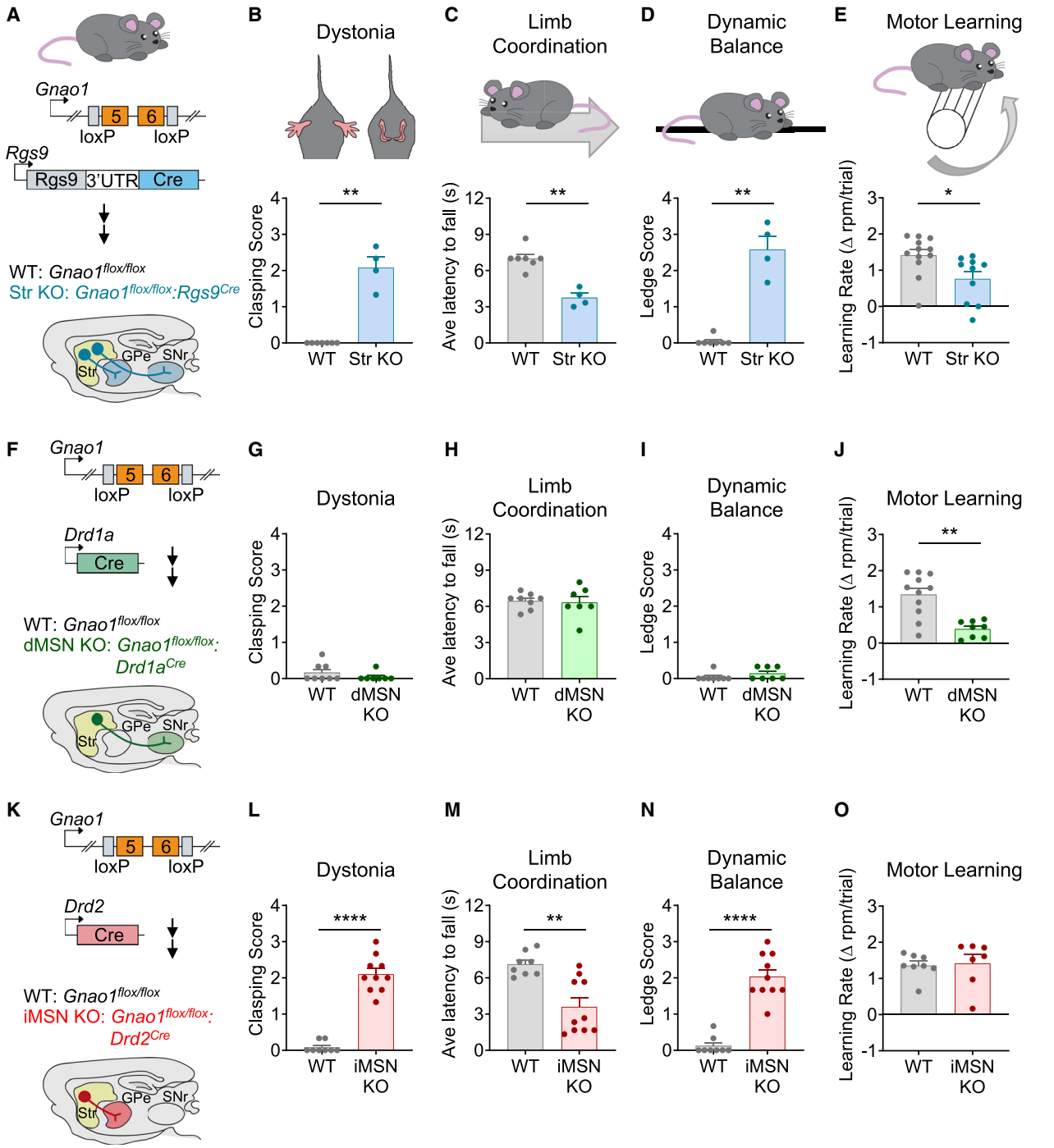

Figure 1. *Gnao1* expression in dMSNs required for motor learning in mice

(A) Schematic of targeting *Gnao1* deletion in striatal neurons.

(B) Hindlimb clasping pathology score for $Gnao1^{flox/flox}$ (WT; n = 7) and $Gnao1^{flox/flox}$:$RGS9^{Cre}$ (Str KO; n = 4) mice (nonparametric t test p = 0.0030, Kolmogorov-Smirnov D = 1.000).

(C) Latency to fall off a rotating beam while walking backward for $Gnao1^{flox/flox}$ (WT; n = 7) and $Gnao1^{flox/flox}$:$RGS9^{Cre}$ (Str KO; n = 4) mice (nonparametric t test p = 0.0030, Kolmogorov-Smirnov D = 1.000).

(D) Ledge test pathology score for $Gnao1^{flox/flox}$ (WT; n = 7) and $Gnao1^{flox/flox}$:$RGS9^{Cre}$ (Str KO; n = 4) mice (nonparametric t test p = 0.0030, Kolmogorov-Smirnov D = 1.000).

(E) Accelerating rotarod learning rate for $Gnao1^{flox/flox}$ (WT; n = 12) and $Gnao1^{flox/flox}$:$RGS9^{Cre}$ (Str KO; n = 10) mice (nonparametric t test p = 0.0157, Kolmogorov-Smirnov D = 0.6667).

(legend continued on next page)

2017). Knockin mouse models carrying orthologous mutations to clinical variants in Gαo recapitulate movement dysregulation phenotypes (Feng et al., 2019; Larrivee et al., 2019). Furthermore, pathogenic Gαo mutants show deficits in cAMP regulation in heterologous cellular assays (Feng et al., 2017). However, the mechanistic basis of this disorder and the functional effects of GNAO1-causing mutations on GPCR signaling in an endogenous setting are unknown.

In this study, we establish the role of Gαo in neuromodulatory control of striatal circuitry and movement in mice. By recording cAMP dynamics in individual neuronal populations using real-time optical sensors, we defined the contribution of Gαo in processing dopamine and adenosine signals. We further delineated underlying signaling mechanisms in cell-based and enzymatic biochemical assays. On the basis of these findings, we probed how pathogenic mutations causing the *GNAO1* disorder affect G protein signaling, neuron function, and behavior leading to functional classification of disease mechanisms. Together, our findings resolve the mechanistic role Gαo plays in controlling GPCR signaling to cAMP and demonstrate how its disruption manifests in disease.

RESULTS

Gαo acts in striatal neurons to enable coordination of movements

The striatum is a key brain structure for motor control implicated in the pathophysiology of many movement disorders (Giordano et al., 2018). To begin probing the role of Gαo in movement, we ablated Gαo specifically in the striatum by crossing mice containing a conditional *Gnao1*$^{flox/flox}$ allele with the pan-striatal driver line *Rgs9*^{cre} (Figures 1A and S1A). The resulting *Gnao1*$^{flox/flox}$*:RGS9*^{Cre} striatal knockout (Str KO) animals were viable and fertile and did not show gross hyperactivity (Figures S1B and S1C) reported in the global knockout (Jiang et al., 1998).

We assessed motor functions of Str KO mice and their wild-type (WT) littermates (*Gnao1*$^{flox/flox}$) in a panel of neurological tests. When evaluating dystonia features, we found that in contrast to normal outward hindlimb extension by WT mice, Str KO clasped their hindlimbs inward to the abdomen (Figure 1B). The Str KO animals also showed profound deficits when challenged to coordinate their movement sequences when walking backward on a rotating beam (Figure 1C). Similarly, the Str KO displayed ineffective hindlimb use in the ledge test when compared to the WT littermates (Figure 1D). The performance of Str KO mice was also significantly reduced in both vertical and horizontal pole tests (Figures S1D and S1E), indicating impairments in coordination and balance.

Finally, we probed the role of Gαo in the acquisition and retention of motor skills using accelerated rotarod. This test revealed that Str KO mice had significantly reduced improvements in performance compared with WT when assayed across multiple consecutive trials (Figures 1E and S1F). The motor learning impairment in Str KO animals persisted over prolonged periods of time (Figures S1G–S1I). Importantly, the observed motor deficits were not due to physical inability, as both genotypes had equal grip strength (Figure S1J).

The striatum contains two populations of medium spiny neurons (MSNs) characterized by divergent projection sites and differential expression of dopamine receptor subtypes: Drd1-expressing direct-pathway neurons (dMSNs) and Drd2-expressing indirect-pathway neurons (iMSNs) (Gerfen et al., 1990). Synchronized activity between these two neuronal populations is thought to coordinate motor programs (Jin et al., 2014; Tecuapetla et al., 2014, 2016). Therefore, we next sought to determine the identity of striatal output neurons requiring Gαo for motor control. First, we eliminated Gαo selectively in dMSNs (dMSN KO) by crossing *Gnao1*$^{flox/flox}$ with a *Drd1a*^{Cre} driver line (Figure 1F and S1A). Assessment of dystonic features in dMSN KO revealed no differences in hindlimb clasping score compared to WT littermates (Figure 1G). The dMSN KO mice also performed similarly as WT littermates during the backward walking challenge (Figure 1H), ledge test (Figure 1I), vertical pole climb (Figure S1K), and horizontal pole assay (Figure S1L). Interestingly, dMSN KO phenocopied only the motor learning deficits observed in Str KO mice, showing a significantly decreased performance on rotarod relative to WT littermates (Figures S1M and 1J). Grip strength was again similar between genotypes (Figure S1N), and motor learning deficits persisted over extended period of time similar to what was observed in Str KO (Figures S1O–S1Q).

(F) Schematic of targeting *Gnao1* deletion in dMSNs.
(G) Hindlimb clasping pathology score for *Gnao1*$^{flox/flox}$ (WT; n = 8) and *Gnao1*$^{flox/flox}$*:Drd1a*^{Cre} (dMSN KO; n = 7) mice (p = 0.5692, Kolmogorov-Smirnov D = 0.2321).
(H) Latency to fall off a rotating beam while walking backward for *Gnao1*$^{flox/flox}$ (WT; n = 8) and *Gnao1*$^{flox/flox}$*:Drd1a*^{Cre} (dMSN KO; n = 7) mice (nonparametric t test p = 0.6476, Kolmogorov-Smirnov D = 0.3214).
(I) Ledge test pathology score for *Gnao1*$^{flox/flox}$ (WT; n = 7) and *Gnao1*$^{flox/flox}$*:Drd1a*^{Cre} (dMSN KO; n = 8) mice (nonparametric t test p = 0.2821, Kolmogorov-Smirnov D = 0.3036).
(J) Accelerating rotarod learning rate for *Gnao1*$^{flox/flox}$ (WT; n = 11) and *Gnao1*$^{flox/flox}$*:Drd1a*^{Cre} (dMSN KO; n = 8) mice (nonparametric t test p = 0.0041, Kolmogorov-Smirnov D = 0.8182).
(K) Schematic of targeting *Gnao1* deletion in iMSNs.
(L) Hindlimb clasping pathology score for *Gnao1*$^{flox/flox}$ (WT; n = 8) and *Gnao1*$^{flox/flox}$*:Drd2*^{Cre} (iMSN KO; n = 10) mice (p < 0.0001, Kolmogorov-Smirnov D = 1.000).
(M) Latency to fall off a rotating beam while walking backward for *Gnao1*$^{flox/flox}$ (WT; n = 8) and *Gnao1*$^{flox/flox}$*:Drd2*^{Cre} (iMSN KO; n = 10) mice (nonparametric t test p = 0.0012, Kolmogorov-Smirnov D = 0.8000).
(N) Ledge test pathology score for *Gnao1*$^{flox/flox}$ (WT; n = 8) and *Gnao1*$^{flox/flox}$*:Drd2*^{Cre} (iMSN KO; n = 10) mice (nonparametric t test p < 0.0001, Kolmogorov-Smirnov D = 1.000).
(O) Accelerating rotarod learning rate for *Gnao1*$^{flox/flox}$ (WT; n = 8) and *Gnao1*$^{flox/flox}$*:Drd2*^{Cre} (iMSN KO; n = 7) mice (nonparametric t test p = 0.4218, Kolmogorov-Smirnov D = 0.4286). All data are presented as mean ± SEM; *p < 0.05; **p < 0.01; ***p < 0.001; ****p < 0.0001.

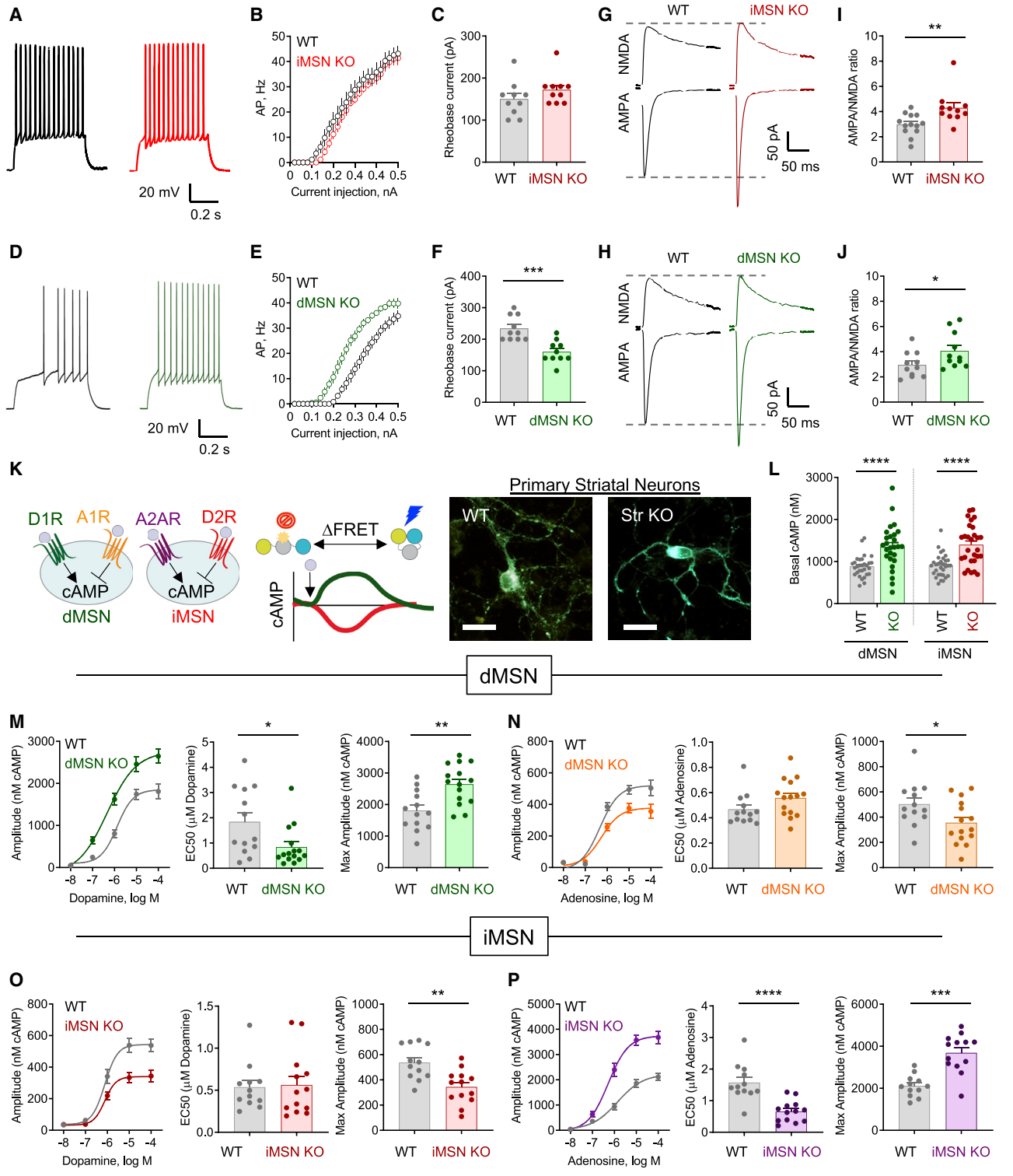

Figure 2. *Gnao1* deletion differentially affects signaling of dMSNs and iMSNs

(A) Representative traces of voltage responses of iMSNs to a depolarizing current step (300 pA) recorded by whole-cell patch clamp from *Drd2*^{Cre} (WT) and *Gnao1*$^{flox/flox}$:*Drd2*^{Cre} (iMSN KO) mice.

(B) Quantification of action potentials elicited in response to somatic current injection in *Drd2*^{Cre} (WT; n = 7 mice/10 neurons) and *Gnao1*$^{flox/flox}$:*Drd2*^{Cre} (iMSN KO; n = 5 mice/10 neurons).

(legend continued on next page)

We next probed the role of Gαo in iMSNs by crossing *Gnao1*$^{flox/flox}$ mice with a *Drd2*^{Cre} driver line (iMSN KO) (Figures 1K and S1A). In contrast to dMSN KO mice, iMSN KO mice phenocopied Str KO across our neurological panel of coordination and balance tests. First, iMSN KO displayed dystonic features, as evidenced by a greater hindlimb clasping score compared to WT littermates (Figure 1L). iMSN KO also showed deficits in the backward walking challenge, ledge test, vertical pole climb, and horizontal pole tests (Figures 1M, 1N, S1R, and S1S) but no motor learning deficits in the rotarod task (Figures S1T and 1O). Together, these findings indicate that striatal Gαo is required for proper motor function differentially programming movements through actions in dMSN and iMSN populations.

Loss of Gαo causes population-specific changes in the activity of striatal neurons and their responses to neuromodulatory inputs

To identify the cellular correlate underlying changes in the motor behavior, we analyzed the activity of striatal neurons by patch-clamp electrophysiology in brain slices. dMSNs and iMSNs were identified by stereotaxic injection of a Cre-dependent adeno-associated virus (AAV) encoding EYFP into dorsomedial striatum of adult mice (Figure S2A). Measurement of intrinsic membrane properties of iMSNs showed no significant alterations in firing properties between iMSN KO (*Gnao1*$^{flox/flox}$:*Drd2*^{Cre}) mice and WT controls (*Drd2*^{Cre}) (Figures 2A–2C). In contrast, dMSN KO (*Gnao1*$^{flox/flox}$:*Drd1a*^{Cre}) neurons had significantly increased excitability, as evidenced by a greater firing frequency (Figures 2D and 2E) and decrease in the rheobase current compared with control (*Drd1a*^{Cre}) (Figure 2F). We observed no changes in other electrophysiological properties of iMSN KO or dMSN KO neurons, including resting membrane potential and input resistance (Figures S2B–S2E). This suggests that the increase in the intrinsic excitability of dMSNs is likely driven by selective molecular alterations.

In addition to changes in intrinsic excitability, alterations in synaptic activity substantially shape actions of striatal neurons. Therefore, we continued to examine the impact of Gαo loss on synaptic properties of dMSNs and iMSNs. Recordings of miniature excitatory postsynaptic currents (mEPSCs) revealed a significant increase in amplitude, but not frequency, in both iMSN KO and dMSN KO (Figures S2F–S2H) consistent with the postsynaptic nature of a change. We next examined the contribution of AMPA receptors (AMPARs) and NMDA receptors (NMDAR) to changes in EPSCs (Figures 2G and 2H). We found that the AMPAR component was significantly increased in both iMSN KO and dMSN KO, whereas the NDMA currents were not significantly changed (Figures S2I and S2J). As a result, deletion of Gαo significantly increased the AMPAR/NMDAR ratio in iMSN KO (Figure 2I) and dMSN KO (Figure 2J). We further ascertained the postsynaptic nature of observed changes by examining the dynamics of dopamine input onto MSNs using cyclic voltammetry and found no changes in evoked dopamine dynamics in either dMSN KO or iMSN KO slices (Figures S2K and S2L). Together, our electrophysiological data indicate that Gαo acts postsynaptically in MSNs to significantly impact synaptic properties of both MSN populations and selectively influence intrinsic excitability of dMSNs.

We next assessed the impact of Gαo on regulation of MSNs by two key neuromodulators in the region, dopamine and

(C) Rheobase current in *Drd2*^{Cre} (WT; n = 7 mice/10 neurons) and *Gnao1*$^{flox/flox}$:*Drd2*^{Cre} (iMSN KO; n = 5 mice/10 neurons) (nonparametric t test; Mann-Whitney test, p = 0.1529).
(D) Representative voltage responses from dMSNs in acute brain slices obtained from *Drd1a*^{Cre} (WT) and *Gnao1*$^{flox/flox}$:*Drd1a2*^{Cre} (dMSN KO).
(E) Quantification of action potentials elicited in response to somatic current injection in *Drd1a*^{Cre} (WT; n = 7 mice/10 neurons) and *Gnao1*$^{flox/flox}$:*Drd1a*^{Cre} (dMSN KO; n = 6 mice/10 neurons).
(F) Rheobase current in *Drd1a*^{Cre} (WT; n = 7 mice/10 neurons) and *Gnao1*$^{flox/flox}$:*Drd1a*^{Cre} (dMSN KO; n = 6 mice/10 neurons) (nonparametric t test; Mann-Whitney test, p = 0.0005).
(G and H) Representative AMPA and NMDA traces obtained from WT, iMSN KO, and dMSN KO.
(I) Quantification of the AMPA/NMDA ratio from *Drd2*^{Cre} (WT; n = 6 mice/13 neurons) and *Gnao1*$^{flox/flox}$:*Drd2*^{Cre} (iMSN KO; n = 6 mice/11 neurons) (nonparametric t test; Mann-Whitney test, p = 0.0048).
(J) Quantification of the AMPA/NMDA ratio from *Drd1a*^{Cre} (WT; n = 6 mice/11 neurons) and *Gnao1*$^{flox/flox}$:*Drd1a*^{Cre} (dMSN KO; n = 5 mice/11 neurons) (nonparametric t test; Mann-Whitney test, p = 0.0473).
(K) Schematic of experimental design and representative images of striatal neurons from *Gnao1*$^{flox/flox}$ (WT) and *Gnao1*$^{flox/flox}$:*RGS9*^{Cre} (Str KO) pups. Scale bar, 20 μm.
(L) Basal cAMP compared between dMSNs from *Gnao1*$^{flox/flox}$ (WT; 30 neurons) and *Gnao1*$^{flox/flox}$:*RGS9*^{Cre} (dMSN KO; 27 neurons), nonparametric t test; Mann-Whitney test, p < 0.0001. Basal cAMP was compared between iMSNs from *Gnao1*$^{flox/flox}$ (WT; 31 neurons) and *Gnao1*$^{flox/flox}$:*RGS9*^{Cre} (iMSN KO; 28 neurons) (nonparametric t test; Mann-Whitney test, p < 0.0001).
(M) Maximum cAMP amplitude to varying doses of dopamine in dMSNs from *Gnao1*$^{flox/flox}$ (WT; n = 13) and *Gnao1*$^{flox/flox}$:*RGS9*^{Cre} (dMSN KO; n = 15) primary striatal neurons; EC_{50} quantification, nonparametric t test; Mann-Whitney test, p = 0.0195; maximum cAMP amplitude to 100-μm dopamine quantification; nonparametric t test; Mann-Whitney test, p = 0.0026).
(N) Maximum cAMP amplitude to varying doses of adenosine in dMSNs from *Gnao1*$^{flox/flox}$ (WT; n = 13) and *Gnao1*$^{flox/flox}$:*RGS9*^{Cre} (dMSN KO; n = 15) primary striatal neurons; EC_{50} quantification, nonparametric t test; Mann-Whitney test, p = 0.0648; maximum cAMP amplitude to 100 μm adenosine quantification; nonparametric t test; Mann-Whitney test, p = 0.0464.
(O) Maximum cAMP amplitude to varying doses of dopamine in iMSNs from *Gnao1*$^{flox/flox}$ (WT; n = 12) and *Gnao1*$^{flox/flox}$:*RGS9*^{Cre} (iMSN KO; n = 13) primary striatal neurons; EC_{50} quantification, nonparametric t test; Mann-Whitney test, p = 0.7689; maximum cAMP amplitude to 100 μm dopamine quantification; nonparametric t test; Mann-Whitney test, p = 0.0016.
(P) Maximum cAMP amplitude to varying doses of adenosine in iMSNs from *Gnao1*$^{flox/flox}$ (WT; n = 12) and *Gnao1*$^{flox/flox}$:*RGS9*^{Cre} (iMSN KO; n = 13) primary striatal neurons; EC_{50} quantification, nonparametric t test; Mann-Whitney test, p < 0.0001; maximum cAMP amplitude to 100 μm adenosine quantification; nonparametric t test; Mann-Whitney test, p = 0.0001.
All data are presented as mean ± SEM; *p < 0.05; **p < 0.01; ***p < 0.001; ****p < 0.0001.

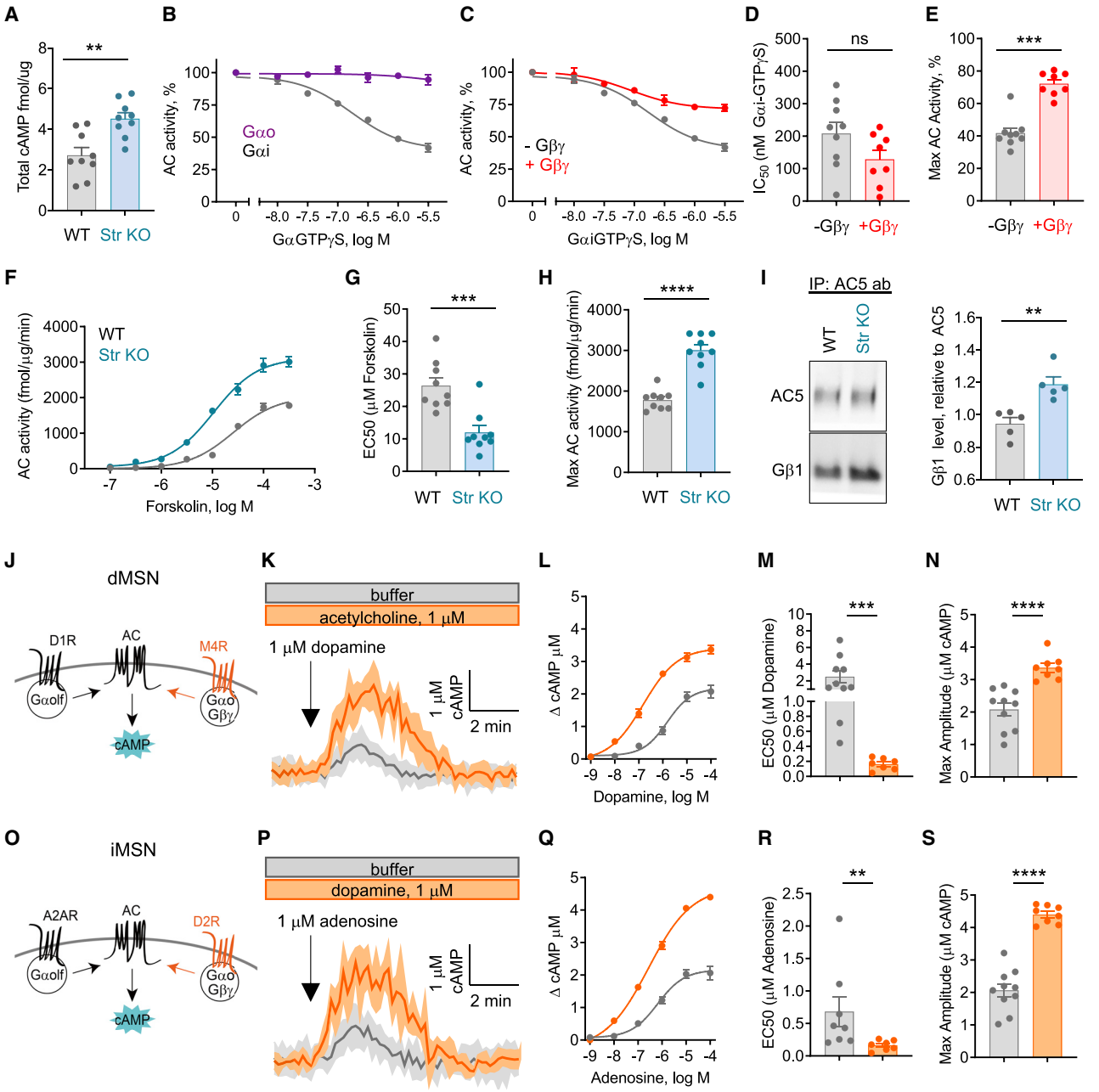

Figure 3. Biochemical mechanism of adenylyl cyclase (AC) regulation by Gαo in the striatum

(A) ELISA determination of total cAMP in striatal tissue punches from *Gnao1*$^{flox/flox}$ (WT; n = 9 mice) and *Gnao1*$^{flox/flox}$*:RGS9*^{Cre} (Str KO; n = 9 mice) (nonparametric t test; Mann-Whitney test, p = 0.0028).

(B) Inhibition of forskolin-stimulated AC in WT striatal membranes by Gαi-GTPγs (n = 8 experiments) or Gαo-GTPγs (n = 3 experiments).

(C) Inhibition of forskolin-stimulated AC in WT striatal membranes by Gαi-GTPγs in the presence of Gβ1γ2 (n = 8 experiments).

(D) IC_{50} to Gαi-GTPγs (n = 8 experiments), nonparametric t test; Mann-Whitney test, p = 0.0927. (E) Efficacy of Gαi-GTPγs inhibition (n = 8 experiments) (nonparametric t test; Mann-Whitney test, p = 0.0002).

(F) Forskolin dose response on striatal membrane AC activity from *Gnao1*$^{flox/flox}$ (WT) and *Gnao1*$^{flox/flox}$*:RGS9*^{Cre} (Str KO) (n = 9 experiments).

(G) EC_{50} to forskolin (n = 9 experiments) (nonparametric t test; Mann-Whitney test, p = 0.0008).

(H) Efficacy of forskolin (n = 9 experiments) (nonparametric t test; Mann-Whitney test, p < 0.0001).

(I) Gβ1 co-immunoprecipitation with anti-AC5 antibody in striatum from *Gnao1*$^{flox/flox}$ (WT; n = 5) and *Gnao1*$^{flox/flox}$*:RGS9*^{Cre} (Str KO; n = 5) mice (nonparametric t test; Mann-Whitney test, p = 0.0079).

(J) Schematic representation of dopamine (D1R) and acetylcholine (M4R) receptor regulation of cAMP in Gαi KO dMSNs.

(K) Dopamine-induced cAMP responses in Gαi KO dMSN in buffer or 1 µM acetylcholine. Data represented as mean ± SD.

(legend continued on next page)

adenosine. Since neuromodulators do not elicit readily recordable changes in the electrophysiological properties of MSNs (Gerfen and Surmeier, 2011), we used an optical strategy (Muntean et al., 2018). We introduced a fluorescence resonance energy transfer (FRET)-based cAMP biosensor into MSNs cultured from neonatal Str KO or WT mice and studied real-time dynamics of cAMP modulation. Segregated expression of dopamine and adenosine receptors enabled the classification of MSNs based on the direction of the cAMP response, which was stimulated by dopamine (via DR1) and decreased by adenosine (via A1R) in dMSNs but inhibited by dopamine (via DR2) and increased by adenosine (via A2AR) in iMSNs (Figure 2K). Initial analysis in Str KO revealed that both dMSNs and iMSNs exhibited significant elevation in cAMP (Figure 2L). In dMSNs, dopamine increased the cAMP signal in a dose-dependent manner (Figure S2M). This relationship had a prominent leftward shift and augmented maximal-response-amplitude neurons (Figure 2M). dMSNs also exhibited a dose-dependent inhibition of cAMP in response to adenosine (Figure S2N). There was no shift in the dose-response of this inhibitory effect; however, these neurons also exhibited reduced maximal response amplitude (Figure 2N). Thus, in dMSN neurons, Gαo affects both the efficacy and potency of responses to dopamine while only modulating adenosine efficacy.

In iMSNs, we found no significant changes in the potency of inhibitory responses to dopamine, and only its efficacy was reduced (Figures 2O and S2O). In contrast, iMSN KO displayed a leftward-shifted dose response following stimulation by adenosine as well as reduction in its maximal amplitude (Figures 2P and S2P). Thus, in iMSN neurons, Gαo affects both efficacy and potency of responses to adenosine while only modulating dopamine efficacy. Taken together, these data indicate that Gαo plays pivotal role in controlling the potency and efficacy of stimulatory neuromodulation while only affecting the efficacy of inhibitory inputs in both populations of striatal neurons.

Gαo tunes efficacy and potency of GPCR signaling to cAMP via Gβγ

To obtain insight into how Gαo drives changes in cAMP induced by the Gαo loss, we analyzed players and reactions involved in this process. First, we confirmed changes in the baseline cAMP levels by biochemical ELISA-based approach. Striatal tissue samples from Str KO animals showed a significant increase in total cAMP levels compared to WT mice (Figure 3A). Western blotting confirmed a significant loss of Gαo in Str KO tissue samples, but no effects on expression of key proteins involved in cAMP generation, such as Gαolf, Gβ2, or AC5 (Figure S3A). Furthermore, Str KO tissues did not show significant effects on levels or activation of kinases affected by dopamine, including Akt, ERK1/2, and GSK3β (Figure S3B). Thus, Str KOs show selective cAMP elevation that is likely driven by alterations in signaling rather than changes in expression of key molecular players.

To determine the mechanisms involved in the effects of Gαo on cAMP production, we turned to biochemical experiments with purified striatal membranes from WT mice. AC5 is the predominant AC isoform in the striatum (Lee et al., 2002), which is directly stimulated by Gαs, inhibited by Gαi, and conditionally stimulated by Gβγ (Gao et al., 2007; Sunahara et al., 1996). We found that purified recombinant Gαo charged with a non-hydrolyzable GTP analog (Gαo-GTPγS) did not significantly affect cAMP production, consistent with previous work showing Gαo does not affect the activity of AC5 (Taussig et al., 1994). In contrast, addition of Gαi-GTPγS readily inhibited cAMP production (Figure 3B). Control experiments confirmed equivalent activity of our recombinant Gαo-GTPγS and Gαi-GTPγS preparations based on their interaction with the Gi/o effector PDE6γ (Figure S3C). These results suggest it is unlikely that the increase in the cAMP levels we see in Gαo KO neurons is due to loss of direct inhibitory influence of Gαo on AC5.

Interestingly, we found that Gβγ subunits effectively reduced the efficacy, but not potency, of the Gαi-mediated inhibitory effect on cAMP production (Figures 3C–3E). This effect is reminiscent of the reduced efficacy of inhibitory cAMP modulation by dopamine in iMSN (via D2R) and adenosine in dMSNs (via A1R). Because Gαo is an effective liberator of functional Gβγ subunits (Digby et al., 2008), it is possible loss of Gαo could result in excess Gβγ signaling activity (Yoda et al., 2015). To test this hypothesis, we compared the AC activities in striatal membrane preparations from WT and Str KO mice. These experiments revealed prominent leftward shift in forskolin dose dependence in Str KO relative to WT (Figures 3F–3H), a hallmark effect produced by Gβγ binding to AC5, sensitizing it to the stimulatory influence of Gαs/olf and forskolin (Gao et al., 2007; Xie et al., 2012). To test the sensitizing effect more directly, we employed biochemical assays stimulating membrane preparations with selective agonists for either D1R (SKF81297; dMSN) or A2AR (CGS21680; iMSN) and measuring the effect on the cAMP production. Indeed, we found significantly greater cAMP production in membranes from Str KO upon activation of D1R or A2R (Figure S3D). Addition of a Gβγ blocker reduced AC5 activity,

(L) Maximum cAMP amplitude to varying doses of dopamine in Gαi KO dMSN in buffer (n = 10 neurons/dose) or 1 μM acetylcholine (n ≥ 6 neurons/dose).
(M) EC_{50} quantification to Gαi KO dMSNs in buffer (n = 10 neurons/dose) or 1 μM acetylcholine (n ≥ 6 neurons/dose) (nonparametric t test; Mann-Whitney test, p = 0.0001).
(N) Maximum cAMP amplitude to 100 μm dopamine in buffer (n = 10 neurons) or 1 μM acetylcholine (n = 8 neurons) (nonparametric t test; Mann-Whitney test, p < 0.0001).
(O) Schematic representation of adenosine (A2AR) and dopamine (D2R) receptor regulation of cAMP in Gαi KO iMSNs.
(P) Adenosine-induced cAMP responses in Gαi KO iMSN in buffer or 1 μM dopamine. Data represented as mean ± SD.
(Q) Maximum cAMP amplitude to varying doses of adenosine in Gαi KO iMSN in buffer (n = 10 neurons/dose) or 1 μM dopamine (n ≥ 5 neurons/dose).
(R) EC_{50} quantification to Gαi KO iMSN in buffer (n = 10 neurons/dose) or 1 μM dopamine (n ≥ 5 neurons/dose) (nonparametric t test; Mann-Whitney test, p = 0.0059).
(S) Maximum cAMP amplitude to 100 μm adenosine in buffer (n = 10 neurons) or 1 μM acetylcholine (n = 8 neurons) (nonparametric t test; Mann-Whitney test, p < 0.0001).
Unless indicated otherwise, all data are presented as mean ± SEM; *p < 0.05; **p < 0.01; ***p < 0.001; ****p < 0.0001.

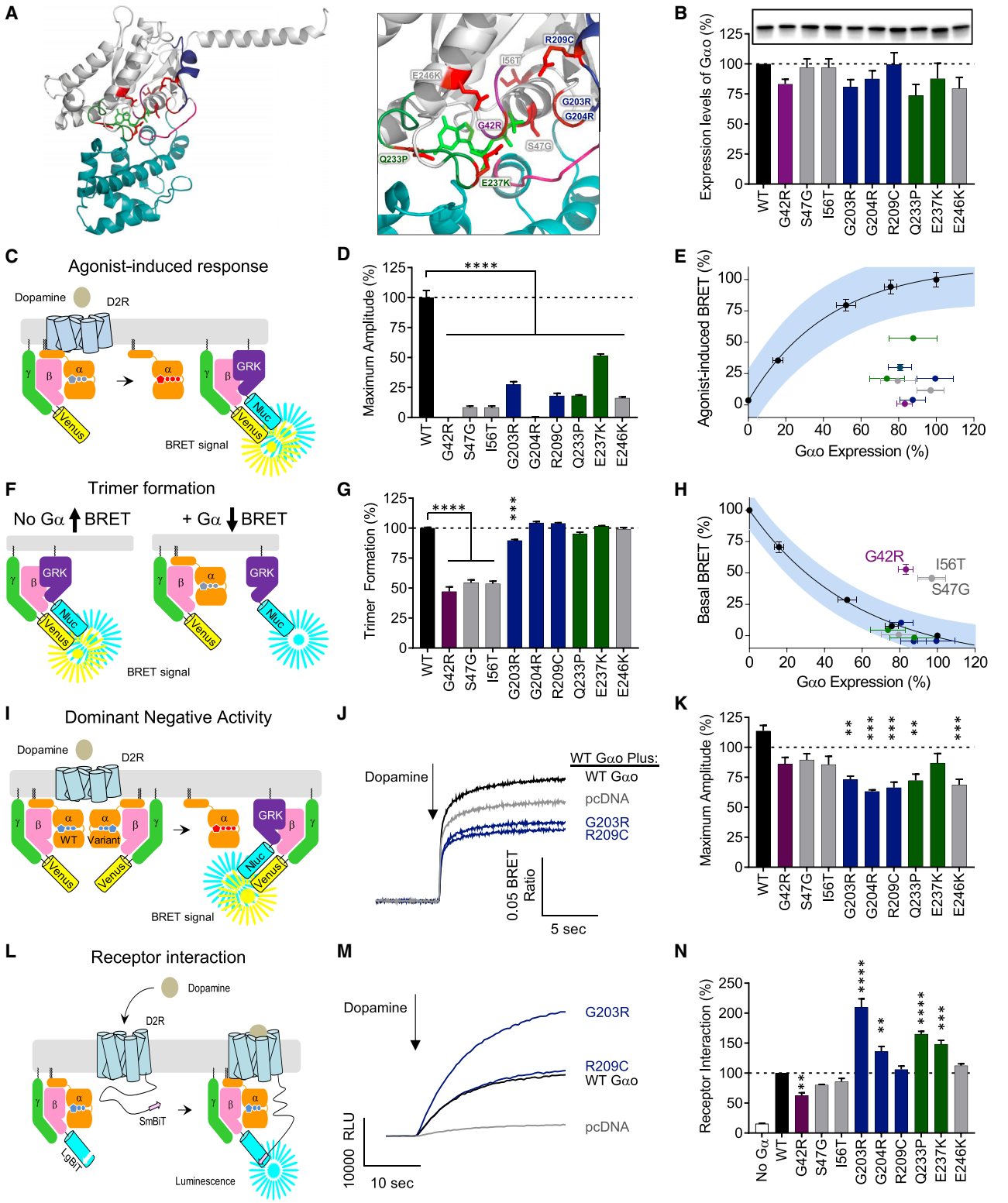

Figure 4. Dissection of pathological mechanisms of *GNAO1* clinical variants

(A) Mapping the genetic variation on the structural model of Gαo. The homology model of Gαo was constructed on the basis of the crystal structure of the Gαi1 (1GP2).

(B) Expression levels of Gαo mutants analyzed by western blotting with anti-Gαo antibody.

(legend continued on next page)

producing a rightward shift in the dose-response curve to stimulation by recombinant Gαs-GTPγS while completely reversing response augmentation in Str KO membranes back to WT levels (Figures S3E and S3F). To probe the biochemical mechanism further, we immunoprecipitated AC5 from striatal tissue and determined its association with Gβγ. We observed significantly increased interaction of Gβ1 with AC5 from Str KO tissue as compared to WT controls (Figure 3I). Collectively, biochemical data support the mechanism whereby Gαo modulates AC5 responsiveness to stimulatory Gαs/olf inputs by controlling the release of Gβγ.

Next, we probed the implications of Gαo-mediated sensitization of AC5 on processing of stimulatory GPCR inputs to cAMP production. In these experiments, we studied how concurrent GPCR-driven activation of Gαo influences stimulatory cAMP responses in MSNs. To do this, we isolated Gαo channel by eliminating Gαi proteins that inhibit AC5 and thus substantially complicate interpretations. We confirmed that CRISPR-Cas9-mediated ablation of all Gαi isoforms eliminated neurotransmitter-mediated suppression of cAMP (Figures S3G and 3H). The lack of cAMP response despite the presence of Gαo in these experiments also fortified our conclusions that Gαo does not inhibit activity of AC5 in striatal neurons. Using this system, we probed how activation of Gαo via Gi/o-coupled GPCRs influences signaling of Gs/olf-coupled GPCRs to cAMP. In dMSNs, we studied the impact of cholinergic modulation mediated by muscarinic M4 receptor (M4R), a Gi/o GPCR prominently expressed in dMSNs (Hersch et al., 1994), on processing of stimulatory D1R-mediated dopamine signals (Figure 3J). Cholinergic inputs provide a major source for regulation of MSN activity (Lim et al., 2014), thus making M4R activation physiologically relevant for examining the interplay between Gαo and Gαolf inputs onto AC5. We found that preincubation of neurons with acetylcholine significantly enhanced the cAMP response to dopamine (Figure 3K). Acetylcholine exposure increased both the potency and efficacy of the stimulatory cAMP response to dopamine (Figures 3L–3N and S3I) as expected from sensitizing effect of Gαo on Gαolf-mediated AC5 stimulation.

In iMSNs, we focused on examining the influence of D2R-mediated activation of Gαo on stimulatory responses to adenosine mediated by A2AR (Figure 3O). Similar to before, dopamine preincubation greatly enhanced cAMP production in response to adenosine (Figure 3P). Again, dopamine exposure increased both the potency and efficacy of the stimulatory cAMP response to adenosine (Figures 3Q–3S and S3I).

Collectively, these results indicate that Gαo controls cAMP production by modulating the levels of Gβγ bound to AC5, which enhances efficacy and potency of the stimulatory cAMP influence while reducing efficacy of the inhibitory influence of GPCRs on cAMP generation.

GNAO1-disorder-associated mutations in Gαo disrupt signaling by several mechanisms

In light of the elucidated role of Gαo in regulating signaling to cAMP and motor coordination, we next investigated the impact of several mutations in Gαo associated with *GNAO1* encephalopathy (Kelly et al., 2019; Mihalek et al., 2017) using our recently developed molecular deconvolution platform (Masuho et al., 2018). Structural modeling showed that these mutations mapped to highly conserved motifs among the Gα protein family residing predominantly around the phosphate-binding loop (P loop), switch II, and switch III regions (Figure 4A), suggesting potential influence on Gαo activation (Bosch et al., 2012) and its interaction with guanine nucleotides (Nakamura et al., 2013).

Western blotting of transfected HEK293 cell lysates showed that all Gαo mutants tested were expressed at levels similar to WT Gαo, indicating that mutations did not significantly compromise protein folding and/or stability (Figure 4B). We next assessed the functional activity of Gαo mutants based on their ability to propagate signals using D2R as a model GPCR. Using the bioluminescence resonance transfer (BRET) strategy that monitors G protein activation (Figure 4C), we observed a

(C) The assay design for GPCR-G protein coupling. HEK293T/17 cells were transfected with plasmids encoding FLAG-D2R, Gαo, Venus-Gβ1γ2, and masGRK3ct-Nluc-hemagglutinin (HA). Dopamine application to the transfected cells induces the dissociation of Gαo from Venus-Gβ1γ2, which increases the BRET ratio through the interaction of Venus-Gβ1γ2 with masGRK3ct-Nluc-HA.
(D) Effect of mutations on GPCR-mediated G protein activation.
(E) Correlation analysis of GPCR-mediated G protein activation and Gαo expression levels.
(F) The assay design for trimer formation. In the absence of exogenous Gα subunit, transfected masGRK3ct-Nluc-HA and Venus-Gβ1γ2 produces masGRK3ct-Nluc-HA-bound Venus-Gβ1γ2 and results in high basal BRET signal (left). Exogenous expression of Gαo sequesters Venus-Gβ1γ2 from masGRK3ct-Nluc and decreases the BRET signal (right).
(G) Effect of mutations on trimer formation measured by basal BRET ratio. The ratio obtained without Gαo or with WT Gαo is designated as 0% or 100% trimer formation.
(H) Correlation analysis of trimer formation versus Gαo expression level quantified from western blotting experiments.
(I) The assay design for the dominant-negative activity of Gαo mutants. WT Gαo and mutant Gαo were transfected with FLAG-D2R and BRET sensors. Dominant-negative mutants can suppress the coupling of D2R and WT Gαo.
(J) Time course of agonist-mediated G protein activation. The condition transfected with empty vector, pcDNA3.1(+), mimics a single null allele (gray). The lower activity than this condition indicates the dominant-negative activity of Gα mutants.
(K) Effect of mutations on agonist-mediated G protein activation. The activity of the Gα mutants was compared to the single null allele condition.
(L) The assay design for agonist-induced GPCR-G protein interaction. HEK293T/17 cells were transfected with plasmids encoding D2R-myc-SmBiT, Gαo, LgBiT-Gβ1, and Gγ2. Dopamine application to the transfected cells induces the interaction between dopamine-activated D2R-myc-SmBiT and Go trimer consisted of exogenous Gαo, LgBiT-Gβ1, and Gγ2, resulting in reconstitution of functional Nluc.
(M) Time course of agonist-induced D2R and Gαo interaction.
(N) Effect of mutations on agonist-induced D2R and Gαo interaction (n = 3 experiments).
Statistical analyses were performed by one-way ANOVA followed by the Dunnett's post hoc comparisons with a control. Values represent means ± SEM from three independent experiments, each performed with three replicates. *p < 0.05; **p < 0.01; ***p < 0.001; ****p < 0.0001.

significantly reduced maximum response amplitude in each mutant compared to WT Gαo when D2R was activated by dopamine (Figure 4D). Two mutants, G42R and G204R, completely failed to respond to dopamine application, while others exhibited a range of deficiencies. Correlation of Gαo expression levels with the maximum BRET amplitudes (Figure 4E) confirmed that all mutants show loss of the signaling capacity regardless of their expression levels.

We further examined the effects of representative mutations in both the P loop (G42R) and switch regions (G203R and R209C) on D2R-catalyzed G protein activation using a bimolecular strategy that monitors heterotrimer dissociation directly via changes in BRET between NanoLuc-tagged Gαo and the Venus-tagged Gβγ (Figure S4A). We found that all three mutations resulted in a significantly decreased level of trimer dissociation (Figures S4B and S4C) confirming the data with the indirect Gβγ-release measurements. These observations indicate that all Gαo mutants have impaired activation by GPCRs.

To understand what deficits in G protein cycle underlie the observed loss of signaling we examined the heterotrimeric complex formation of each mutant Gαo with Gβγ. We used the same Gβγ-release BRET assay but measured a suppression of the baseline signal upon introduction of exogenous Gαo (Figure 4F). We found that mutations proximal to the P loop (G42R, S47G, and I56T) resulted in prominent deficits in Gβγ binding. G203R led to small but significant reduction in signal (Figure 4G). When trimer formation was corrected for fluctuations in expression levels, we found that only G42R, S47G and I56T mutants significantly affected Gβγ binding compared to WT Gαo (Figure 4H). Thus, association with Gβγ is only compromised by mutations in the P loop of Gαo.

The dominant nature of *GNAO1* disorder implies that mutant proteins are expressed alongside a WT Gαo copy. Therefore, we next tested Gαo variants for the interference with the dopamine responses of WT Gαo (Figure 4I). We found that five switch region mutants (G203R, G204R, R209C, Q233P, E246K) significantly suppressed BRET responses indicating that they interfere with D2R-mediated activation of the WT Gαo (Figures 4J and 4K). To assess how these dominant-negative effects occur, we developed an assay to measure association of G protein heterotrimers with the D2R. This approach relies on complementation between SmBit-tagged D2R and LgBit-tagged Gβγ, producing luminescent NLuc upon interaction (Figure 4L). We found that all Gαo mutants showed agonist-induced recruitment to D2R. Strikingly, several mutants with dominant-negative activity (G203R, G204R, and Q233P) showed a significant increase in D2R association, suggesting that their interfering effects on signaling could be caused by increased, nonproductive interactions with GPCRs (Figures 4M and 4N). Overall, these results revealed that pathogenic variants in Gαo exhibit a spectrum of effects ranging in severity along two principal axes, loss in the ability to transmit GPCR signals and dominant-negative blockade of signaling.

GNAO1-disorder-associated mutations in Gαo cause neuron-type-specific impairment in cAMP signaling in striatal neurons

To understand the relevance of observed signaling deficits in Gαo mutants to the processing of motor commands, we evaluated how these mutations affect signaling in MSNs. We chose two of the most prevalent Gαo variants that also feature prominent effects on signaling observed in reconstituted studies, G203R (dominant negative with strong GPCR trapping) and R209C (dominant negative without increased GPCR association). The mutants were introduced into neurons cultured from *Gnao1*$^{flox/flox}$ mice containing WT Gαo to better model the heterozygosity situation occurring in the brains of *GNAO1* patients. Dose-response studies were performed to evaluate the effects on both potency and efficacy of signaling (Figures 5A, 5E, S5A, and S5C). Strikingly, these studies revealed that Gαo mutants produced unique effects differentially impacting dopamine signaling in a MSN-subtype-selective fashion (Figures 5B and 5F). The R209C mutant affected iMSN responses exclusively, lowering the efficacy of dopamine signaling. In contrast, the G203R mutant affected both populations increasing potency of the response in dMSN and lowering efficacy in iMSNs.

These changes were mirrored by alterations in adenosine responses (Figures 5C, 5G, S5B, and S5D). Here, the R209C mutation affected dMSN exclusively, diminishing the efficacy of adenosine signaling (Figures 5D and 5H). In contrast, G203R mutation affected both populations, reducing efficacy in dMSNs while increasing potency of adenosine responses in iMSNs (Figures 5D and 5H). In summary, these experiments indicate that dominant-negative Gαo mutants cause cell-type-selective interference with processing of dopamine and adenosine signals by striatal neurons.

Dominant-negative GNAO1 variants disrupt motor control upon expression in individual populations of striatal neurons

Our studies indicate that several pathological Gαo mutations have dominant-negative activity that impairs transmission of neuromodulatory signals involved in motor control. To ascertain the implications of these observations for animal behavior *in vivo*, we expressed two *GNAO1* variants with dominant-negative activity in different populations of striatal neurons followed by evaluation of mice in our neurological panel of motor behaviors. This was accomplished by stereotaxic delivery of Cre-dependent AAV particles encoding *GNAO1* variants in the dorsal striatum of adult *Drd1*^{Cre} and *Drd2*^{Cre} mice (Figure 6A). The strategy enables expression of Gαo mutants alongside the WT copy, thus resembling the pathological situation in patients with GNAO1 disorder.

We first assessed spontaneous dystonia by scoring clasping behavior. Expression of WT Gαo did not influence hindlimb clasping, whereas expression of either G203R or R209C in either dMSNs and iMSNs resulted in a significant clasping (Figure 6B). Expression of either the G203R or R209C variant, but not WT Gαo, also significantly reduced the limb coordination of mice assessed by the backward walking task (Figure 6C). Similarly, we found that expression of either G203R or R209C mutants, but not WT Gαo, in either MSN population significantly compromised balance and coordination in the ledge test (Figure 6D) as well as in the vertical and horizontal pole tests (Figures S6A and S6B). Finally, we assessed motor learning utilizing the rotarod (Figure 6E). None of the mutants, expressed in either MSN population, differed from WT Gαo in their ability to stay

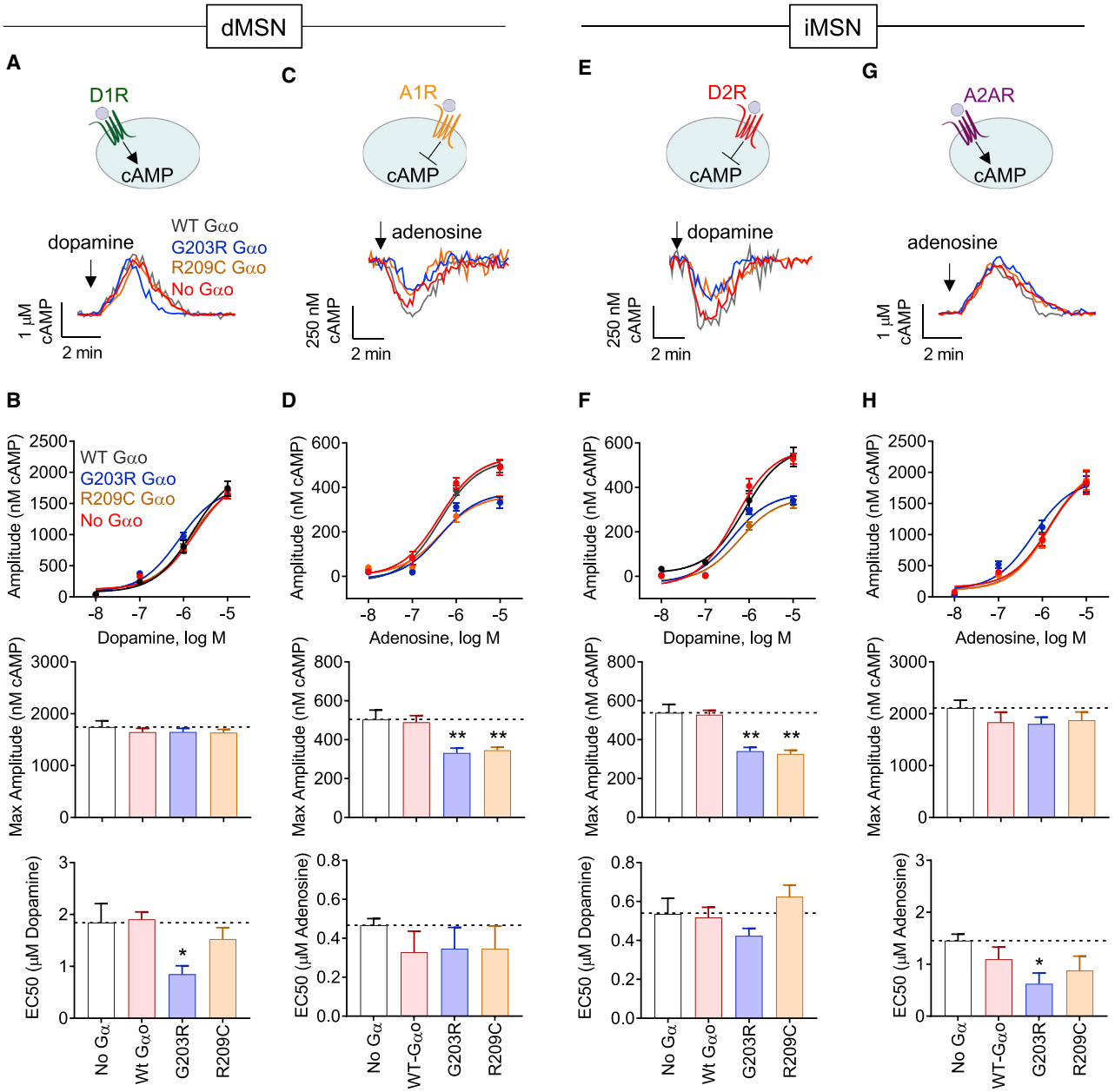

Figure 5. *GNAO1* genetic variants impart circuit-specific alterations in striatal dopamine and adenosine signal integration

(A) Mean cAMP response to 10 μM dopamine in *Gnao1*$^{flox/flox}$ dMSNs transfected with indicated Gαo variant.

(B) *Gnao1*$^{flox/flox}$ dMSNs transfected with indicated Gαo dose-response curve to dopamine (top), quantification of maximum cAMP amplitude to 10 μM dopamine (middle), and EC_{50} to dopamine (bottom). n (# neurons) = no Gα (13), WT Gαo (10), G203R (8), R209C (10).

(C) Mean cAMP response to 10 μM adenosine in *Gnao1*$^{flox/flox}$ dMSNs transfected with indicated Gαo variant.

(D) *Gnao1*$^{flox/flox}$ dMSNs transfected with indicated Gαo dose-response curve to adenosine (top), quantification of maximum cAMP amplitude to 10 μM adenosine (middle), and EC_{50} to adenosine (bottom). n (# neurons) = no Gα (13), WT Gαo (12), G203R (13), R209C (14).

(E) Mean cAMP response to 10 μM dopamine in *Gnao1*$^{flox/flox}$ iMSNs transfected with indicated Gαo.

(F) *Gnao1*$^{flox/flox}$ iMSNs transfected with indicated Gαo dose-response curve to dopamine (top), quantification of maximum cAMP amplitude to 10 μM dopamine (middle), and EC_{50} to dopamine (bottom). n (# neurons) = no Gα (12), WT Gαo (6), G203R (8), R209C (7).

(G) Mean cAMP response to 10 μM adenosine in *Gnao1*$^{flox/flox}$ iMSNs transfected with indicated Gαo.

(H) *Gnao1*$^{flox/flox}$ iMSNs transfected with indicated Gαo dose-response curve to adenosine (top), quantification of maximum cAMP amplitude to 10 μM adenosine (middle), and EC_{50} to adenosine (bottom). n (# neurons) = no Gα (12), WT Gαo (13), G203R (12), R209C (13).

All data are presented as mean ± SEM; one-way ANOVA, Holm-Sidak's multiple comparisons test; *p < 0.05; **p < 0.01; ***p < 0.001; ****p < 0.0001.

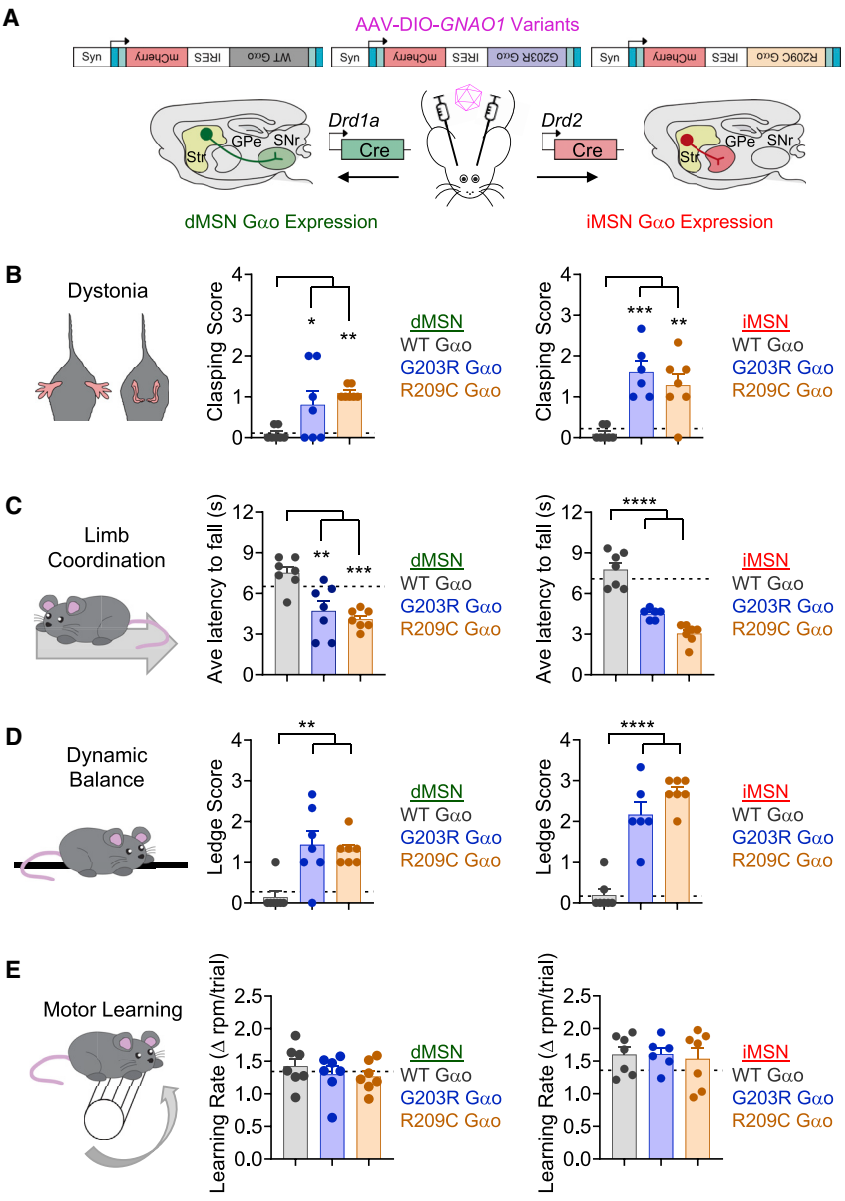

Figure 6. *GNAO1* mutations impair locomotor behavior in mice

(A) Schematic of targeting expression of *GNAO1* variants (G203R, R209C, or WT control) in defined striatal neurons by stereotaxic delivery of Cre-dependent AAV in either adult $Drd1a^{Cre}$ (dMSN Gαo expression) or $Drd2^{Cre}$ (iMSN Gαo expression) mice.

(B) Hindlimb clasping pathology score for $Drd1a^{Cre}$ mice expressing WT Gαo (n = 7), G203R Gαo (n = 7), or R209C Gαo (n = 7) (one-way ANOVA, Dunnett's multiple comparisons test; WT versus G203R p = 0.0414, WT versus R209C p = 0.0050), and hindlimb clasping pathology score for $Drd2^{Cre}$ mice expressing WT Gαo (n = 7), G203R Gαo (n = 6), or R209C Gαo (n = 7) (one-way ANOVA, Dunnett's multiple comparisons test; WT versus G203R p = 0.0003, WT versus R209C p = 0.0021).

(C) Latency to fall off a rotating beam while walking backward for $Drd1a^{Cre}$ mice expressing WT Gαo (n = 7), G203R Gαo (n = 7), or R209C Gαo (n = 7) (one-way ANOVA, Dunnett's multiple comparisons test; WT versus G203R p = 0.0019, WT versus R209C p = 0.0003), and latency to fall off a rotating beam while walking backward for $Drd2^{Cre}$ mice expressing WT Gαo (n = 7), G203R Gαo (n = 6), or R209C Gαo (n = 7) (one-way ANOVA, Dunnett's multiple comparisons test; WT versus G203R p < 0.0001, WT versus R209C p < 0.0001).

(D) Ledge test pathology score for $Drd1a^{Cre}$ mice expressing WT Gαo (n = 7), G203R Gαo (n = 7), or R209C Gαo (n = 7) (one-way ANOVA, Dunnett's multiple comparisons test; WT versus G203R p = 0.0015, WT versus R209C p = 0.0041), and ledge test pathology score for $Drd2^{Cre}$ mice expressing WT Gαo (n = 7), G203R Gαo (n = 6), or R209C Gαo (n = 7) (one-way ANOVA, Dunnett's multiple comparisons test; WT versus G203R p < 0.0001, WT versus R209C p < 0.0001).

(E) Accelerating rotarod learning rate for $Drd1a^{Cre}$ mice expressing WT Gαo (n = 7), G203R Gαo (n = 7), or R209C Gαo (n = 7) (one-way ANOVA, Dunnett's multiple comparisons test; WT versus G203R p = 0.6411, WT versus R209C p = 0.5076), and accelerating rotarod learning rate for $Drd2^{Cre}$ mice expressing WT Gαo (n = 7), G203R Gαo (n = 6), or R209C Gαo (n = 7) (one-way ANOVA, Dunnett's multiple comparisons test; WT versus G203R p = 0.9979, WT versus R209C p = 0.9093). All data are presented as mean ± SEM; *p < 0.05; **p < 0.01; ***p < 0.001; ****p < 0.0001.

on the rotarod or improve their rate of learning over 3 days (Figure S6C). Based on these results, we conclude that the dominant-negative influence of G203R and R209C variants in either MSN subpopulation is sufficient to disrupt signaling that leads to profound movement control deficits.

DISCUSSION

Role of Gαo in canonical GPCR signaling to cAMP

A number of studies demonstrated key roles of neuromodulators acting on distinct GPCRs at discrete points in striatal circuitry in shaping behavioral outcomes related to action selection and reward programming (Castro and Bruchas, 2019; Kravitz and Kreitzer, 2012; Lovinger, 2010). However, the role of individual G protein signals initiated by these inputs remains poorly defined. The key contribution of this study is defining the role of Gαo in controlling canonical GPCR signaling to cAMP in striatal neurons (Figure 7A). By examining endogenous GPCR signaling in striatal neurons, we found that Gαo prominently impacts processing of both stimulatory and inhibitory inputs. In accord with previous observations (Wong et al., 1992), we found that Gαo does not directly regulate cAMP-producing activity of AC5 in striatal membranes. Our investigation revealed that Gαo regulates cAMP production by controlling the availability of Gβγ for AC5 binding. This impacts the processing of inputs onto AC5 in two

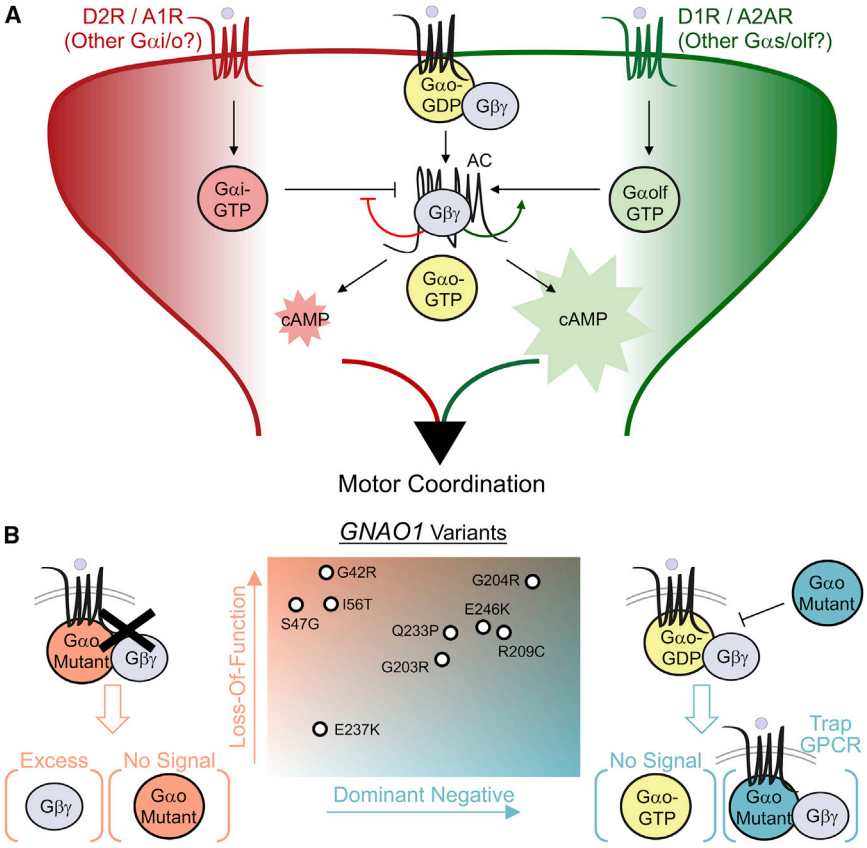

Figure 7. Model of Gαo mechanism in processing of GPCR signals to cAMP and its alteration by pathogenic GNAO1 mutations

(A) Canonical role of Gαo acting as signaling modifier through regulation of Gβγ. By interacting with an allosteric site on AC5, Gβγ increases the potency of Gαs/olf stimulation and diminishes efficacy of Gαi-mediated inhibition. This results in reducing inhibitory tone of Gαi inputs while sensitizing Gαolf stimulation of AC5 in striatal neurons.

(B) *GNAO1* clinical variants manifest a spectrum of pathology through individualized strength in scaled loss-of-function (LOF) and dominant-negative (DN) properties.

ways. First, it increases the potency of stimulatory responses causing the leftward shift on dopamine dose dependence, consistent with a previously noted sensitizing effect of Gβγ on Gαs/olf-mediated stimulation of AC5 (Gao et al., 2007). This would allow the neurons to titrate the sensitivity of their stimulatory inputs that trigger cAMP production based on the level of Gαo activation. Second, Gβγ, when complexed with AC5, diminishes the efficacy of inhibitory Gαi-mediated regulation. This would allow the neurons to scale the volume of cAMP response depending on the extent of Gαo activation. Thus, although not directly regulating AC activity, Gαo nevertheless appears to be a critical modifier of cAMP responsiveness to GPCR activation, fine-tuning the processing of signals by Gαi and Gαs/olf. We envision that this mechanism could operate in a number of neuron types affecting signaling by a number of GPCRs and scale the cAMP response efficacy and potency depending upon signaling demands. From a broader perspective, this puts forward a model in which GPCRs engage Gαo to open an additional communication channel that instructs response modification across several receptors in parallel to the main signaling modality.

Function of Gαo in striatal neurotransmission and motor control

The striatum is one of the key brain regions involved in coordination of movements (Liljeholm and O'Doherty, 2012). Dopamine signaling is well known to exert profound effects on motor control (Baik et al., 1995; Xu et al., 1994; Zhai et al., 2019). Recent evidence also points to involvement of Gαo in dopamine receptor function in the striatum (Jiang et al., 2001; Marcott et al., 2018). Our results demonstrate that Gαo function in the striatum is critical for multiple aspects of movement control. We found that Gαo is selectively required in iMSNs, but not dMSNs, for balance and coordination. This aligns with the role of dMSNs in promoting action selection (i.e., motor learning) (Hikida et al., 2010) as opposed to iMSNs adjusting complex action sequences (i.e., motor coordination) by inhibition of competing motor programs (Tecuapetla et al., 2016). Indeed, when we deleted Gαo in iMSNs, we observed severe deficits in limb coordination and spatial balance. Gαo is prominently activated by D2R signaling (Jiang et al., 2001), suggesting it could play a role at high levels of dopamine signaling above the dynamic range achieved upon motor learning. In line with this, we found that Gαo is needed for achieving high efficacy of D2R-mediated responses to dopamine without affecting the response sensitivity in iMSN, thus further supporting a role for iMSNs in coordination. Indeed, targeted D2R pharmacology has remained a therapeutic approach to treat early coordination deficits in Parkinson's disease patients for many years (Lewis et al., 2006).

Finally, we found that loss of Gαo in iMSNs was responsible for inducing dystonia-like features often observed *GNAO1* patients (Mihalek et al., 2017), which could be considered a part of hyperkinetic motor program constrained by this neuronal population (Durieux et al., 2009). The selective involvement of Gαo supports a dominant role of iMSN circuitry in dystonia (Berardelli et al., 1998), including observed alterations in electrophysiological properties of iMSNs in mouse models of dystonia (Sciamanna et al., 2020). In this connection, it is also interesting to note that deep brain stimulation of the external global pallidus, a major projection site of iMSNs (Gerfen et al., 1990), improves motor epochs in primary dystonia patients (Houeto et al., 2007).

Our observations introduce Gαo in the genetic network of players in striatal neurons that are essential for motor function

in both human disease and mouse models. Pathogenic mutations in the stimulatory striatal G protein Gαolf (encoded by *GNAL*) cause dystonia (Fuchs et al., 2013), while *Gnal* haploinsufficiency in mice impairs motor learning (Pelosi et al., 2017). The Gβγ subunits also play critical roles in movement as observed in patients with Gβ1 mutation (Lohmann et al., 2017) and Gγ7 KO mice (Schwindinger et al., 2003). Movement disorder is also associated with *ADCY5* mutations (OMIM: 606703), and again, motor learning deficits are observed in AC5 KO mice (Iwamoto et al., 2003; Kheirbek et al., 2009). Finally, striatal PDE10A is associated with motor deficits in patients (OMIM: 616921) and mice (Siuciak et al., 2006). In addition to these players, which are all important elements in the GPCR-cAMP axis, our findings that Gαo affects cAMP homeostasis bolsters the case that striatal cAMP signaling is critical for motor control (Qian et al., 2015).

Molecular mechanisms of GNAO1 movement disorder

Our evaluation of Gαo variants that cause GNAO1 disorder provides insights into mechanisms underlying pathological signal processing. All GNAO1 variants that we tested displayed a loss-of-function (LOF) behavior in transmission of GPCR signals. We found that these deficits arose from distinct mechanisms affecting G protein cycle, including impairment in binding to Gβγ and inability to promote downstream signaling. In addition, several mutants displayed clear dominant-negative effects interfering with the function of the normal Gαo. Many of these effects are not mutually exclusive and show a spectrum of the severities. Thus, on the basis of these observations, we propose a model that GNAO1 mutations disrupt GPCR signaling through a combination of two principal mechanisms, loss of signaling ability and dominant-negative interference (Figure 7B).

Our conclusions regarding molecular mechanisms underlying disruption in Gαo function are supported by a wealth of structural, biochemical, and mutagenesis studies on the function of conserved elements shared by all G protein α subunits. For example, mutations in the P loop region (G42R, S47G, and I56T) affect nucleotide binding due to steric interference (Bosch et al., 2012; Natochin et al., 2006; Raw et al., 1997; Slepak et al., 1993a; 1995; Yu et al., 1996). Similarly, alterations in switch II (G203R, G204R, and R209C) are not tolerated because this region on the Gα subunits contains key catalytic sites (Sprang, 2016). Steric substitutions in this motif may prevent achieving an active conformational state induced by GTP binding, as observed in several G proteins (Inoue et al., 1995; Osawa and Johnson, 1991; Slepak et al., 1993a, 1993b; Thomas et al., 2004). Finally, many of these alterations were also previously noted to produce dominant-negative effects, supporting the idea that deficits in the G protein cycle and receptor trapping may be intimately linked (Natochin et al., 2006; Slepak et al., 1993a, 1995).

Our observations contradict the findings from a recent survey of *GNAO1* mutations that classified variants as LOF, gain of function (GOF), or normal function (NF) based on their ability to suppress cAMP production in reconstituted cellular systems (Feng et al., 2017). Several considerations may explain this discrepancy. First, the effects of GNAO1-related mutations were previously studied in combination with the C351G point mutation engineered to impart pertussis toxin (PTX) insensitivity. This mutation alters the C-terminal region critical for GPCR engagement (Flock et al., 2017). As a result, this manipulation might have altered signaling outcomes, which could be particularly relevant in the case of dominant-negative variants that we show in many cases are explained by enhanced GPCR interactions. Given our results that Gαo affects cAMP production indirectly, mutation of the C-terminal region and concomitant inactivation of endogenous proteins by PTX may have also led to artificial outcomes due to cross-talk in complex signaling network that regulates AC activity. Finally, the proposed classification makes it unclear how Gαo variants with no detectable deficits (NF) contribute to an established disease pathology. Our results indicate that one such mutation, R209C, previously considered NF, in fact results in LOF accompanied by a dominant-negative activity at the levels of signaling, neuronal function, and mouse behavior.

Intriguingly, our findings indicate that different GNAO1-disorder-associated mutations in Gαo affect processing of neuromodulatory signals in a neuron-type-specific manner depending on the type of mutation. For example, the R209C mutation disrupts inhibitory signals and thus selectively skews iMSN responses to dopamine and dMSN responses to adenosine. The G203R mutation has strong dominant-negative activity perturbing integration of dopamine and adenosine in both dMSNs and iMSNs. This implies that each *GNAO1* variant likely adjusts signaling pressure in a unique manner to misalign striatal coordination and imbalance motor control (Figure 7). Thus, disease variants likely produce circuit-selective effects depending on the particular mechanisms of their signaling disruptions. This would inherently generate diversity in the adverse outcome stemming from different variations in Gαo. In accordance with the range of severity in movement disorders observed in *GNAO1* patients (Kelly et al., 2019), we suggest that the pathology is a continuous spectrum rather than isolated manifestations. As such, we believe phenotype-genotype correlations in GNAO1 disorder are likely quite nuanced and need to take into account the exact mechanisms of individual causal mutations on a case-by-case basis. Indeed, a recent review of the clinical data suggests a substantial overlap in disease symptoms across patients carrying different variants (~80% of patients) (Schirinzi et al., 2019). The findings we describe here on the molecular and cellular effects of Gαo mutations are likely to be valuable for informing our understanding of the pathology of GNAO1 encephalopathy and individualized pharmacotherapies to treat this disorder.

STAR★METHODS

Detailed methods are provided in the online version of this paper and include the following:

- KEY RESOURCES TABLE
- RESOURCE AVAILABILITY
  - Lead contact

SUPPLEMENTAL INFORMATION

Supplemental Information can be found online at https://doi.org/10.1016/j.celrep.2021.108718.

ACKNOWLEDGMENTS

We thank Natalia Martemyanova for husbandry, maintenance, and genotyping of all the mice examined in this study, as well as Nickolas K. Skamangas and Hideko Masuho for technical support. This work was supported by funding from the NIH (grants DA041207 to B.S.M., DA048579 to S.Z., NS072129 to B.G., and DA036596 and DA026405 to K.A.M.) and the Intramural Research Program of the NIH (project Z01-ES-101643 to L.B.). This work was also supported by a research fellowship from the Bow Foundation (B.S.M.).

AUTHOR CONTRIBUTIONS

B.S.M. designed and performed all imaging experiments, analyzed the data, and wrote the paper; L.P.S. and M.D. designed and performed all behavioral experiments and analyzed the data; I.M. designed and performed the experiments analyzing effects of clinical mutations in cell-based assays and analyzed the data; S.Z. designed and performed all electrophysiological experiments and analyzed the data; D.W. and B.G. were involved in analysis of mutation mechanisms; D.N.P. generated critical reagent (recombinant proteins); L.B. generated critical reagent (*Gnao1*^{fx} mice); B.G. and R.D.B. participated in writing the manuscript; H.I. performed voltammetry studies; K.A.M. conceived the study, designed experiments, analyzed the data, and wrote the paper with feedback from all authors; and all authors participated in editing the manuscript.

DECLARATION OF INTERESTS

The authors declare no competing interests.

Received: October 17, 2019
Revised: December 7, 2020
Accepted: January 11, 2021
Published: February 2, 2021

REFERENCES

Ananth, A.L., Robichaux-Viehoever, A., Kim, Y.M., Hanson-Kahn, A., Cox, R., Enns, G.M., Strober, J., Willing, M., Schlaggar, B.L., Wu, Y.W., and Bernstein, J.A. (2016). Clinical course of six children with GNAO1 mutations causing a severe and distinctive movement disorder. Pediatr. Neurol. *59*, 81–84.

Arshavsky, V.Y., Dumke, C.L., Zhu, Y., Artemyev, N.O., Skiba, N.P., Hamm, H.E., and Bownds, M.D. (1994). Regulation of transducin GTPase activity in bovine rod outer segments. J. Biol. Chem. *269*, 19882–19887.

Baik, J.H., Picetti, R., Saiardi, A., Thiriet, G., Dierich, A., Depaulis, A., Le Meur, M., and Borrelli, E. (1995). Parkinsonian-like locomotor impairment in mice lacking dopamine D2 receptors. Nature *377*, 424–428.

Berardelli, A., Rothwell, J.C., Hallett, M., Thompson, P.D., Manfredi, M., and Marsden, C.D. (1998). The pathophysiology of primary dystonia. Brain *121*, 1195–1212.

Betke, K.M., Wells, C.A., and Hamm, H.E. (2012). GPCR mediated regulation of synaptic transmission. Prog. Neurobiol. *96*, 304–321.

Bjarnadóttir, T.K., Gloriam, D.E., Hellstrand, S.H., Kristiansson, H., Fredriksson, R., and Schiöth, H.B. (2006). Comprehensive repertoire and phylogenetic analysis of the G protein-coupled receptors in human and mouse. Genomics *88*, 263–273.

Bosch, D.E., Willard, F.S., Ramanujam, R., Kimple, A.J., Willard, M.D., Naqvi, N.I., and Siderovski, D.P. (2012). A P-loop mutation in Gα subunits prevents transition to the active state: implications for G-protein signaling in fungal pathogenesis. PLoS Pathog. *8*, e1002553.

Campbell, V., Berrow, N., and Dolphin, A.C. (1993). GABAB receptor modulation of Ca2+ currents in rat sensory neurones by the G protein G(0): antisense oligonucleotide studies. J. Physiol. *470*, 1–11.

Castro, D.C., and Bruchas, M.R. (2019). A motivational and neuropeptidergic hub: anatomical and functional diversity within the nucleus accumbens shell. Neuron *102*, 529–552.

Celver, J., Sharma, M., and Kovoor, A. (2012). D(2)-Dopamine receptors target regulator of G protein signaling 9-2 to detergent-resistant membrane fractions. J. Neurochem. *120*, 56–69.

Chamero, P., Katsoulidou, V., Hendrix, P., Bufe, B., Roberts, R., Matsunami, H., Abramowitz, J., Birnbaumer, L., Zufall, F., and Leinders-Zufall, T. (2011). G protein G(alpha)o is essential for vomeronasal function and aggressive behavior in mice. Proc. Natl. Acad. Sci. USA *108*, 12898–12903.

Corvol, J.C., Studler, J.M., Schonn, J.S., Girault, J.A., and Hervé, D. (2001). Galpha(olf) is necessary for coupling D1 and A2a receptors to adenylyl cyclase in the striatum. J. Neurochem. *76*, 1585–1588.

Dang, M.T., Yokoi, F., Yin, H.H., Lovinger, D.M., Wang, Y., and Li, Y. (2006). Disrupted motor learning and long-term synaptic plasticity in mice lacking NMDAR1 in the striatum. Proc. Natl. Acad. Sci. USA *103*, 15254–15259.

Dessauer, C.W. (2002). Kinetic analysis of the action of P-site analogs. Methods Enzymol. *345*, 112–126.

Digby, G.J., Sethi, P.R., and Lambert, N.A. (2008). Differential dissociation of G protein heterotrimers. J. Physiol. *586*, 3325–3335.

Doyle, T.B., Muntean, B.S., Ejendal, K.F., Hayes, M.P., Soto-Velasquez, M., Martemyanov, K.A., Dessauer, C.W., Hu, C.D., and Watts, V.J. (2019). Identification of novel adenylyl cyclase 5 (AC5) signaling networks in D_1 and D_2 medium spiny neurons using bimolecular fluorescence complementation screening. Cells *8*, 1468.

Durieux, P.F., Bearzatto, B., Guiducci, S., Buch, T., Waisman, A., Zoli, M., Schiffmann, S.N., and de Kerchove d'Exaerde, A. (2009). D2R striatopallidal neurons inhibit both locomotor and drug reward processes. Nat. Neurosci. *12*, 393–395.

Ewald, D.A., Pang, I.H., Sternweis, P.C., and Miller, R.J. (1989). Differential G protein-mediated coupling of neurotransmitter receptors to Ca2+ channels in rat dorsal root ganglion neurons in vitro. Neuron *2*, 1185–1193.

Farr, T.D., Liu, L., Colwell, K.L., Whishaw, I.Q., and Metz, G.A. (2006). Bilateral alteration in stepping pattern after unilateral motor cortex injury: a new test strategy for analysis of skilled limb movements in neurological mouse models. J. Neurosci. Methods *153*, 104–113.

Feng, H., Sjögren, B., Karaj, B., Shaw, V., Gezer, A., and Neubig, R.R. (2017). Movement disorder in *GNAO1* encephalopathy associated with gain-of-function mutations. Neurology *89*, 762–770.

Feng, H., Larrivee, C.L., Demireva, E.Y., Xie, H., Leipprandt, J.R., and Neubig, R.R. (2019). Mouse models of GNAO1-associated movement disorder: Allele- and sex-specific differences in phenotypes. PLoS ONE *14*, e0211066.

Flock, T., Hauser, A.S., Lund, N., Gloriam, D.E., Balaji, S., and Babu, M.M. (2017). Selectivity determinants of GPCR-G-protein binding. Nature *545*, 317–322.

Fuchs, T., Saunders-Pullman, R., Masuho, I., Luciano, M.S., Raymond, D., Factor, S., Lang, A.E., Liang, T.W., Trosch, R.M., White, S., et al. (2013). Mutations in GNAL cause primary torsion dystonia. Nat. Genet. *45*, 88–92.

Gao, X., Sadana, R., Dessauer, C.W., and Patel, T.B. (2007). Conditional stimulation of type V and VI adenylyl cyclases by G protein betagamma subunits. J. Biol. Chem. *282*, 294–302.

Gerfen, C.R., and Surmeier, D.J. (2011). Modulation of striatal projection systems by dopamine. Annu. Rev. Neurosci. *34*, 441–466.

Gerfen, C.R., Engber, T.M., Mahan, L.C., Susel, Z., Chase, T.N., Monsma, F.J., Jr., and Sibley, D.R. (1990). D1 and D2 dopamine receptor-regulated gene expression of striatonigral and striatopallidal neurons. Science *250*, 1429–1432.

Ghahremani, M.H., Cheng, P., Lembo, P.M., and Albert, P.R. (1999). Distinct roles for Galphai2, Galphai3, and Gbeta gamma in modulation offorskolin- or Gs-mediated cAMP accumulation and calcium mobilization by dopamine D2S receptors. J. Biol. Chem. *274*, 9238–9245.

Gilman, A.G. (1987). G proteins: transducers of receptor-generated signals. Annu. Rev. Biochem. *56*, 615–649.

Giordano, N., Iemolo, A., Mancini, M., Cacace, F., De Risi, M., Latagliata, E.C., Ghiglieri, V., Bellenchi, G.C., Puglisi-Allegra, S., Calabresi, P., et al. (2018). Motor learning and metaplasticity in striatal neurons: relevance for Parkinson's disease. Brain *141*, 505–520.

Guyenet, S.J., Furrer, S.A., Damian, V.M., Baughan, T.D., La Spada, A.R., and Garden, G.A. (2010). A simple composite phenotype scoring system for evaluating mouse models of cerebellar ataxia. J. Vis. Exp. *39*, 1787.

Håkansson, K., Lindskog, M., Pozzi, L., Usiello, A., and Fisone, G. (2004). DARPP-32 and modulation of cAMP signaling: involvement in motor control and levodopa-induced dyskinesia. Parkinsonism Relat. Disord. *10*, 281–286.

Hersch, S.M., Gutekunst, C.A., Rees, H.D., Heilman, C.J., and Levey, A.I. (1994). Distribution of m1-m4 muscarinic receptor proteins in the rat striatum: light and electron microscopic immunocytochemistry using subtype-specific antibodies. J. Neurosci. *14*, 3351–3363.

Hikida, T., Kimura, K., Wada, N., Funabiki, K., and Nakanishi, S. (2010). Distinct roles of synaptic transmission in direct and indirect striatal pathways to reward and aversive behavior. Neuron *66*, 896–907.

Hollins, B., Kuravi, S., Digby, G.J., and Lambert, N.A. (2009). The c-terminus of GRK3 indicates rapid dissociation of G protein heterotrimers. Cell. Signal. *21*, 1015–1021.

Houeto, J.L., Yelnik, J., Bardinet, E., Vercueil, L., Krystkowiak, P., Mesnage, V., Lagrange, C., Dormont, D., Le Bas, J.F., Pruvo, J.P., et al.; French Stimulation du Pallidum Interne dans la Dystonie Study Group (2007). Acute deep-brain stimulation of the internal and external globus pallidus in primary dystonia: functional mapping of the pallidum. Arch. Neurol. *64*, 1281–1286.

Inoue, S., Hoshino, S., Kukimoto, I., Ui, M., and Katada, T. (1995). Purification and characterization of the G203T mutant alpha i-2 subunit of GTP-binding protein expressed in baculovirus-infected Sf9 cells. J. Biochem. *118*, 650–657.

Iwamoto, T., Okumura, S., Iwatsubo, K., Kawabe, J., Ohtsu, K., Sakai, I., Hashimoto, Y., Izumitani, A., Sango, K., Ajiki, K., et al. (2003). Motor dysfunction in type 5 adenylyl cyclase-null mice. J. Biol. Chem. *278*, 16936–16940.

Jiang, M., Gold, M.S., Boulay, G., Spicher, K., Peyton, M., Brabet, P., Srinivasan, Y., Rudolph, U., Ellison, G., and Birnbaumer, L. (1998). Multiple neurological abnormalities in mice deficient in the G protein Go. Proc. Natl. Acad. Sci. USA *95*, 3269–3274.

Jiang, M., Spicher, K., Boulay, G., Wang, Y., and Birnbaumer, L. (2001). Most central nervous system D2 dopamine receptors are coupled to their effectors by Go. Proc. Natl. Acad. Sci. USA *98*, 3577–3582.

Jin, X., Tecuapetla, F., and Costa, R.M. (2014). Basal ganglia subcircuits distinctively encode the parsing and concatenation of action sequences. Nat. Neurosci. *17*, 423–430.

Kandel, E.R. (2012). The molecular biology of memory: cAMP, PKA, CRE, CREB-1, CREB-2, and CPEB. Mol. Brain *5*, 14.

Kelly, M., Park, M., Mihalek, I., Rochtus, A., Gramm, M., Pérez-Palma, E., Axeen, E.T., Hung, C.Y., Olson, H., Swanson, L., et al.; Undiagnosed Diseases Network (2019). Spectrum of neurodevelopmental disease associated with the GNAO1 guanosine triphosphate-binding region. Epilepsia *60*, 406–418.

Kheirbek, M.A., Britt, J.P., Beeler, J.A., Ishikawa, Y., McGehee, D.S., and Zhuang, X. (2009). Adenylyl cyclase type 5 contributes to corticostriatal plasticity and striatum-dependent learning. J. Neurosci. *29*, 12115–12124.

Klarenbeek, J.B., Goedhart, J., Hink, M.A., Gadella, T.W., and Jalink, K. (2011). A mTurquoise-Based cAMP Sensor for Both FLIM and Ratiometric Read-Out Has Improved Dynamic Range. PLoS One *6*, e19170.

Kravitz, A.V., and Kreitzer, A.C. (2012). Striatal mechanisms underlying movement, reinforcement, and punishment. Physiology (Bethesda) *27*, 167–177.

Larrivee, C.L., Feng, H., Quinn, J.A., Shaw, V.S., Leipprandt, J.R., Demireva, E.Y., Xie, H., and Neubig, R.R. (2019). Mice with *GNAO1* R209H movement disorder variant display hyperlocomotion alleviated by risperidone. bioRxiv. https://doi.org/10.1124/jpet.119.262733.

Lee, E., Linder, M.E., and Gilman, A.G. (1994). Expression of G-protein alpha subunits in Escherichia coli. Methods Enzymol. *237*, 146–164.

Lee, K.W., Hong, J.H., Choi, I.Y., Che, Y., Lee, J.K., Yang, S.D., Song, C.W., Kang, H.S., Lee, J.H., Noh, J.S., et al. (2002). Impaired D2 dopamine receptor function in mice lacking type 5 adenylyl cyclase. J. Neurosci. *22*, 7931–7940.

Lee, B.Y., Thulin, C.D., and Willardson, B.M. (2004). Site-specific phosphorylation of phosducin in intact retina. Dynamics of phosphorylation and effects on G protein beta gamma dimer binding. J. Biol. Chem. *279*, 54008–54017.

Lewis, M.M., Huang, X., Nichols, D.E., and Mailman, R.B. (2006). D1 and functionally selective dopamine agonists as neuroprotective agents in Parkinson's disease. CNS Neurol. Disord. Drug Targets *5*, 345–353.

Liljeholm, M., and O'Doherty, J.P. (2012). Contributions of the striatum to learning, motivation, and performance: an associative account. Trends Cogn. Sci. *16*, 467–475.

Lim, S.A., Kang, U.J., and McGehee, D.S. (2014). Striatal cholinergic interneuron regulation and circuit effects. Front. Synaptic Neurosci. *6*, 22.

Lohmann, K., Masuho, I., Patil, D.N., Baumann, H., Hebert, E., Steinrücke, S., Trujillano, D., Skamangas, N.K., Dobricic, V., Hüning, I., et al. (2017). Novel GNB1 mutations disrupt assembly and function of G protein heterotrimers and cause global developmental delay in humans. Hum. Mol. Genet. *26*, 1078–1086.

Lovinger, D.M. (2010). Neurotransmitter roles in synaptic modulation, plasticity and learning in the dorsal striatum. Neuropharmacology *58*, 951–961.

Marcott, P.F., Gong, S., Donthamsetti, P., Grinnell, S.G., Nelson, M.N., Newman, A.H., Birnbaumer, L., Martemyanov, K.A., Javitch, J.A., and Ford, C.P. (2018). Regional heterogeneity of D2-receptor signaling in the dorsal striatum and nucleus accumbens. Neuron *98*, 575–587.e4.

Masuho, I., Martemyanov, K.A., and Lambert, N.A. (2015a). Monitoring G protein activation in cells with BRET. Methods Mol. Biol. *1335*, 107–113.

Masuho, I., Ostrovskaya, O., Kramer, G.M., Jones, C.D., Xie, K., and Martemyanov, K.A. (2015b). Distinct profiles of functional discrimination among G proteins determine the actions of G protein-coupled receptors. Sci. Signal. *8*, ra123.

Masuho, I., Chavali, S., Muntean, B.S., Skamangas, N.K., Simonyan, K., Patil, D.N., Kramer, G.M., Ozelius, L., Babu, M.M., and Martemyanov, K.A. (2018). Molecular deconvolution platform to establish disease mechanisms by surveying GPCR signaling. Cell Rep. *24*, 557–568.e5.

Matsuura, K., Kabuto, H., Makino, H., and Ogawa, N. (1997). Pole test is a useful method for evaluating the mouse movement disorder caused by striatal dopamine depletion. J. Neurosci. Methods *73*, 45–48.

Mihalek, I., Park, M., Kelly, M., Waugh, J.L., Poduri, A., and Bodamer, O. (2017). Molecular map of GNAO1-related disease phenotypes and reactions to treatment. biorxiv.

Muntean, B.S., Zucca, S., MacMullen, C.M., Dao, M.T., Johnston, C., Iwamoto, H., Blakely, R.D., Davis, R.L., and Martemyanov, K.A. (2018). Interrogating the spatiotemporal landscape of neuromodulatory GPCR signaling by real-time imaging of cAMP in intact neurons and circuits. Cell Rep. *22*, 255–268.

Nakamura, K., Kodera, H., Akita, T., Shiina, M., Kato, M., Hoshino, H., Terashima, H., Osaka, H., Nakamura, S., Tohyama, J., et al. (2013). De novo mutations in GNAO1, encoding a Gαo subunit of heterotrimeric G proteins, cause epileptic encephalopathy. Am. J. Hum. Genet. *93*, 496–505.

Natochin, M., Barren, B., and Artemyev, N.O. (2006). Dominant negative mutants of transducin-alpha that block activated receptor. Biochemistry *45*, 6488–6494.

Orlandi, C., Sutton, L.P., Muntean, B.S., Song, C., and Martemyanov, K.A. (2019). Homeostatic cAMP regulation by the RGS7 complex controls depression-related behaviors. Neuropsychopharmacology *44*, 642–653.

Osawa, S., and Johnson, G.L. (1991). A dominant negative G alpha s mutant is rescued by secondary mutation of the alpha chain amino terminus. J. Biol. Chem. *266*, 4673–4676.

Pelosi, A., Menardy, F., Popa, D., Girault, J.A., and Hervé, D. (2017). Heterozygous Gnal mice are a novel animal model with which to study dystonia pathophysiology. J. Neurosci. *37*, 6253–6267.

Pierce, K.L., Premont, R.T., and Lefkowitz, R.J. (2002). Seven-transmembrane receptors. Nat. Rev. Mol. Cell Biol. *3*, 639–650.

Purvanov, V., Koval, A., and Katanaev, V.L. (2010). A direct and functional interaction between Go and Rab5 during G protein-coupled receptor signaling. Sci. Signal. *3*, ra65.

Qian, Y., Forssberg, H., and Diaz Heijtz, R. (2015). Motor skill learning is associated with phase-dependent modifications in the striatal cAMP/PKA/DARPP-32 signaling pathway in rodents. PLoS ONE *10*, e0140974.

Raw, A.S., Coleman, D.E., Gilman, A.G., and Sprang, S.R. (1997). Structural and biochemical characterization of the GTPgammaS-, GDP.Pi-, and GDP-bound forms of a GTPase-deficient Gly42–> Val mutant of Gialpha1. Biochemistry *36*, 15660–15669.

Rice, M.E., Cragg, S.J., and Greenfield, S.A. (1997). Characteristics of electrically evoked somatodendritic dopamine release in substantia nigra and ventral tegmental area in vitro. J. Neurophysiol. *77*, 853–862.

Sadana, R., and Dessauer, C.W. (2009). Physiological roles for G protein-regulated adenylyl cyclase isoforms: insights from knockout and overexpression studies. Neurosignals *17*, 5–22.

Schirinzi, T., Garone, G., Travaglini, L., Vasco, G., Galosi, S., Rios, L., Castiglioni, C., Barassi, C., Battaglia, D., Gambardella, M.L., et al. (2019). Phenomenology and clinical course of movement disorder in GNAO1 variants: Results from an analytical review. Parkinsonism Relat. Disord. *61*, 19–25.

Schwindinger, W.F., Betz, K.S., Giger, K.E., Sabol, A., Bronson, S.K., and Robishaw, J.D. (2003). Loss of G protein gamma 7 alters behavior and reduces striatal alpha(olf) level and cAMP production. J. Biol. Chem. *278*, 6575–6579.

Sciamanna, G., Ponterio, G., Vanni, V., Laricchiuta, D., Martella, G., Bonsi, P., Meringolo, M., Tassone, A., Mercuri, N.B., and Pisani, A. (2020). Optogenetic activation of striatopallidal neurons reveals altered HCN gating in DYT1 dystonia. Cell Rep. *31*, 107644.

Siuciak, J.A., McCarthy, S.A., Chapin, D.S., Fujiwara, R.A., James, L.C., Williams, R.D., Stock, J.L., McNeish, J.D., Strick, C.A., Menniti, F.S., and Schmidt, C.J. (2006). Genetic deletion of the striatum-enriched phosphodiesterase PDE10A: evidence for altered striatal function. Neuropharmacology *51*, 374–385.

Slepak, V.Z., Quick, M.W., Aragay, A.M., Davidson, N., Lester, H.A., and Simon, M.I. (1993a). Random mutagenesis of G protein alpha subunit G(o) alpha. Mutations altering nucleotide binding. J. Biol. Chem. *268*, 21889–21894.

Slepak, V.Z., Wilkie, T.M., and Simon, M.I. (1993b). Mutational analysis of G protein alpha subunit G(o) alpha expressed in Escherichia coli. J. Biol. Chem. *268*, 1414–1423.

Slepak, V.Z., Katz, A., and Simon, M.I. (1995). Functional analysis of a dominant negative mutant of G alpha i2. J. Biol. Chem. *270*, 4037–4041.

Solis, G.P., Bilousov, O., Koval, A., Lüchtenborg, A.M., Lin, C., and Katanaev, V.L. (2017). Golgi-resident Gαo promotes protrusive membrane dynamics. Cell *170*, 939–955.e24.

Sprang, S.R. (2016). Invited review: activation of G proteins by GTP and the mechanism of Gα-catalyzed GTP hydrolysis. Biopolymers *105*, 449–462.

Sternweis, P.C., and Robishaw, J.D. (1984). Isolation of two proteins with high affinity for guanine nucleotides from membranes of bovine brain. J. Biol. Chem. *259*, 13806–13813.

Strittmatter, S.M., Valenzuela, D., Kennedy, T.E., Neer, E.J., and Fishman, M.C. (1990). G0 is a major growth cone protein subject to regulation by GAP-43. Nature *344*, 836–841.

Sunahara, R.K., Dessauer, C.W., and Gilman, A.G. (1996). Complexity and diversity of mammalian adenylyl cyclases. Annu. Rev. Pharmacol. Toxicol. *36*, 461–480.

Sutton, L.P., Ostrovskaya, O., Dao, M., Xie, K., Orlandi, C., Smith, R., Wee, S., and Martemyanov, K.A. (2016). Regulator of G-protein signaling 7 regulates reward behavior by controlling opioid signaling in the striatum. Biol. Psychiatry *80*, 235–245.

Taussig, R., Tang, W.J., Hepler, J.R., and Gilman, A.G. (1994). Distinct patterns of bidirectional regulation of mammalian adenylyl cyclases. J. Biol. Chem. *269*, 6093–6100.

Tecuapetla, F., Matias, S., Dugue, G.P., Mainen, Z.F., and Costa, R.M. (2014). Balanced activity in basal ganglia projection pathways is critical for contraversive movements. Nat. Commun. *5*, 4315.

Tecuapetla, F., Jin, X., Lima, S.Q., and Costa, R.M. (2016). Complementary contributions of striatal projection pathways to action initiation and execution. Cell *166*, 703–715.

Thomas, C.J., Du, X., Li, P., Wang, Y., Ross, E.M., and Sprang, S.R. (2004). Uncoupling conformational change from GTP hydrolysis in a heterotrimeric G protein alpha-subunit. Proc. Natl. Acad. Sci. USA *101*, 7560–7565.

VanDongen, A.M., Codina, J., Olate, J., Mattera, R., Joho, R., Birnbaumer, L., and Brown, A.M. (1988). Newly identified brain potassium channels gated by the guanine nucleotide binding protein Go. Science *242*, 1433–1437.

Wettschureck, N., and Offermanns, S. (2005). Mammalian G proteins and their cell type specific functions. Physiol. Rev. *85*, 1159–1204.

Wolfgang, W.J., Quan, F., Goldsmith, P., Unson, C., Spiegel, A., and Forte, M. (1990). Immunolocalization of G protein alpha-subunits in the Drosophila CNS. J. Neurosci. *10*, 1014–1024.

Wong, Y.H., Conklin, B.R., and Bourne, H.R. (1992). Gz-mediated hormonal inhibition of cyclic AMP accumulation. Science *255*, 339–342.

Xie, K., Masuho, I., Brand, C., Dessauer, C.W., and Martemyanov, K.A. (2012). The complex of G protein regulator RGS9-2 and Gβ(5) controls sensitization and signaling kinetics of type 5 adenylyl cyclase in the striatum. Sci. Signal. *5*, ra63.

Xie, K., Masuho, I., Shih, C.C., Cao, Y., Sasaki, K., Lai, C.W., Han, P.L., Ueda, H., Dessauer, C.W., Ehrlich, M.E., et al. (2015). Stable G protein-effector complexes in striatal neurons: mechanism of assembly and role in neurotransmitter signaling. eLife *4*, e10451.

Xu, M., Moratalla, R., Gold, L.H., Hiroi, N., Koob, G.F., Graybiel, A.M., and Tonegawa, S. (1994). Dopamine D1 receptor mutant mice are deficient in striatal expression of dynorphin and in dopamine-mediated behavioral responses. Cell *79*, 729–742.

Yoda, A., Adelmant, G., Tamburini, J., Chapuy, B., Shindoh, N., Yoda, Y., Weigert, O., Kopp, N., Wu, S.C., Kim, S.S., et al. (2015). Mutations in G protein β subunits promote transformation and kinase inhibitor resistance. Nat. Med. *21*, 71–75.

Yu, J.H., Wieser, J., and Adams, T.H. (1996). The Aspergillus FlbA RGS domain protein antagonizes G protein signaling to block proliferation and allow development. EMBO J. *15*, 5184–5190.

Zhai, S., Shen, W., Graves, S.M., and Surmeier, D.J. (2019). Dopaminergic modulation of striatal function and Parkinson's disease. J. Neural Transm. (Vienna) *126*, 411–422.

STAR★METHODS

KEY RESOURCES TABLE

REAGENT or RESOURCE	SOURCE	IDENTIFIER
Antibodies		
Mouse monoclonal anti-AC5	Xie et al., 2015	N/A
Rabbit polyclonal anti-Gαo	Cell Signaling Technology	3975
Rabbit polyclonal anti-Gαolf	Corvol et al., 2001	N/A
Rabbit polyclonal anti-Gβ1	Lee et al., 2004	N/A
Rabbit polyclonal anti-Gβ2 (C-16)	Santa Cruz Biotechnology	sc-380; RRID:AB_2263466
Rabbit monoclonal anti-phospho-AKT (Ser473) (D9E)	Cell Signaling Technology	4060; RRID:AB_2315049
Mouse monoclonal anti-AKT (pan) (40D4)	Cell Signaling Technology	2920; RRID:AB_1147620
Rabbit polyclonal anti-phospho-Erk1/2 (Thr202/Tyr204)	Cell Signaling Technology	9101; RRID:AB_331646
Rabbit monoclonal anti-Erk1/2 (Ser473) (137F5)	Cell Signaling Technology	4695; RRID:AB_390779
Rabbit monoclonal anti-GSK-3α/β (D75D3)	Cell Signaling Technology	5676
Rabbit polyclonal anti-phospho-GSK-3α/β (Ser21/9)	Cell Signaling Technology	9331; RRID:AB_329830
Chicken polyclonal anti-GAPDH	Millipore Sigma	AB2302; RRID:AB_10615768
Bacterial and virus strains		
Escherichia coli: BL21(DE3) Chemically Competent	Thermo Fisher Scientific	C600003
AAV5-EF1α-DIO-EYFP	UNC Vector Core	N/A
AAV9-Syn-DIO-Gαo WT-IRES-mCherry	VectorBuilder	N/A
AAV9-Syn-DIO-Gαo G203R-IRES-mCherry	VectorBuilder	N/A
AAV9-Syn-DIO-Gαo R209C-IRES-mCherry	VectorBuilder	N/A
Chemicals, peptides, and recombinant proteins		
Dulbecco's modified Eagle's medium	Thermo Fisher Scientific	11965-092
MEM non-essential amino acids	Thermo Fisher Scientific	11140-050
Sodium pyruvate	Thermo Fisher Scientific	11360-070
Penicillin-streptomycin	Thermo Fisher Scientific	15140-122
Fetal bovine serum	Millipore Sigma	12303C
GlutaMAX	Thermo Fisher Scientific	35050-061
Neurobasal-A	Thermo Fisher Scientific	10888-022
DNaseI	Thermo Fisher Scientific	18047019
Papain	Worthington	LS003126
B27 Supplement	Thermo Fisher Scientific	17504044
Hanks' balanced salt solution	Thermo Fisher Scientific	14175-095
Poly-D-Lysine	Millipore Sigma	P6407
Lipofectamine 2000	Thermo Fisher Scientific	11668027
Lipofectamine LTX Reagent with PLUS Reagent	Thermo Fisher Scientific	15338100
cOmplete protease inhibitor	Millipore Sigma	11873580001
IPTG	Goldbio	I2481
Recombinant: Gαo	This paper	N/A
Recombinant: Gαi	Lee et al., 1994	N/A
Recombinant: Gαs	Lee et al., 1994	N/A
Recombinant: Gβ1γ2	Xie et al., 2012	N/A

(*Continued on next page*)

Continued

REAGENT or RESOURCE	SOURCE	IDENTIFIER
Recombinant: His-PDEγ(63-87)	Arshavsky et al., 1994	N/A
Guanosine 5-[γ-thio]triphosphate tetralithium salt	Millipore Sigma	G8634
Ni-NTA Agarose beads	QIAGEN	30210
Bovine serum albumin	VWR	VWRV0332-100G
Pyruvate kinase	Millipore Sigma	P9136
Phosphoenol-pyruvate	Millipore Sigma	10108294001
Adenosine 5-triphosphate disodium salt hydrate	Millipore Sigma	A2383
Guanosine 5-triphosphate sodium salt hydrate	Millipore Sigma	G8877
IBMX	Tocris	2845
Forskolin	Tocris	1099
GRK2i	Tocris	3594
Dopamine hydrochloride	Millipore Sigma	H8502
Adenosine	Millipore Sigma	A4036
Acetylcholine chloride	Tocris	2809
SKF 81297 hydrobromide	Tocris	1447
CGS 21680 hydrochloride	Tocris	1063
Phosphatase Inhibitor Cocktail 2	Millipore Sigma	P5726
Phosphatase Inhibitor Cocktail 3	Millipore Sigma	P0044
C12 E9, non-ionic surfactant	Abcam	ab146545
Dynabeads Protein G	Thermo Fisher Scientific	10004D
Drd1 *in situ* probe	Thermo Fisher Scientific	VB6-12478
Drd2 *in situ* probe	Thermo Fisher Scientific	VB6-16550
Gnao1 exon5_6 *in situ* probe	Thermo Fisher Scientific	VPMFWXD
Critical commercial assays		
Pierce 660nm Protein Assay Reagent	Thermo Fisher Scientific	22660
Direct cAMP ELISA Kit	Enzo Life Sciences	ADI-900-066
Nano-Glo Luciferase Assay Substrate (furimazine)	Promega	N1120
ViewRNA ISH Cell Assay Kit	Thermo Fisher Scientific	QVC0001
Experimental models: cell lines		
Human: HEK293T/17	ATCC	CRL11268
Insect: SF9	Thermo Fisher Scientific	11496015
Experimental models: organisms/strains		
Mouse: Gnao1$^{flox/flox}$	Chamero et al., 2011	N/A
Mouse: Rgs9^{Cre}	Dang et al., 2006	N/A
Mouse: C57BL/6-Tg(Drd1-cre)EY262Gsat/Mmucd	MMRRC	RRID:MMRRC_017264-UCD
Mouse: C57BL/6-Tg(Drd2-cre)ER43Gsat/Mmucd	MMRRC	RRID:MMRRC_017268-UCD
Mouse: C57BL/6-Gt(ROSA)26Sortm1(CAG-ECFP*/Rapgef3/Venus*)Kama/J	Muntean et al., 2018	Jackson Laboratory: 032205
Oligonucleotides		
See Table S2 for oligonucleotide information.	IDT	N/A

(*Continued on next page*)

Continued

REAGENT or RESOURCE	SOURCE	IDENTIFIER
Recombinant DNA		
Plasmid: ^{T}EPAC^{VV}	Klarenbeek et al., 2011	N/A
Plasmid: pcDNA3.1(+)	Thermo Fisher Scientific	V79020
Plasmid: pET28a	Millipore Sigma	69864
Plasmid: human Gαo WT	GenScript	N/A
Plasmid: human Gαo G42R	This Paper	N/A
Plasmid: human Gαo S47G	This Paper	N/A
Plasmid: human Gαo I56T	This Paper	N/A
Plasmid: human Gαo G203R	This Paper	N/A
Plasmid: human Gαo G204R	This Paper	N/A
Plasmid: human Gαo R209C	This Paper	N/A
Plasmid: human Gαo Q233P	This Paper	N/A
Plasmid: human Gαo E237K	This Paper	N/A
Plasmid: human Gαo E246K	This Paper	N/A
Plasmid: Flag-Dopamine D2 Receptor	Celver et al., 2012	N/A
Plasmid: Venus 156-239-Gβ1	Hollins et al., 2009	N/A
Plasmid: Venus 1-155-Gγ2	Hollins et al., 2009	N/A
Plasmid: masGRK3ct-Nluc	Masuho et al., 2015b	N/A
Plasmid: Dopamine D2 Receptor-myc-SmBiT	This paper	N/A
Plasmid: LgBit-Gβ1	This paper	N/A
Plasmid: Human Gγ2	cDNA Resource Center	GNG0200000
Plasmid: human Gαo WT-Nluc	This Paper	N/A
Plasmid: human Gαo G42R-Nluc	This Paper	N/A
Plasmid: human Gαo G203R-Nluc	This Paper	N/A
Plasmid: human Gαo R209C-Nluc	This Paper	N/A
Plasmid: pSECC	Addgene	#60820
Plasmid: pCMV-VSV-G	Addgene	#8454
Plasmid: pMDLg/pRRE	Addgene	#12251
Plasmid: pRSV-Rev	Addgene	#12253
Software and Algorithms		
ImageJ	National Institutes of Health	SCR_003070
Clampfit 10.5	Molecular Devices	SCR_011323
Prism 8	GraphPad	SCR_002798
PyMol	Schrödinger	SCR_000305
Office 365	Microsoft	N/A

RESOURCE AVAILABILITY

Lead contact

Further information and requests for reagents and resources may be directed to, and will be fulfilled by, the Lead Contact, Kirill A. Martemyanov (kirill@scripps.edu).

Materials availability

Constructs generated in this study are available upon request from the Lead Contact.

Data and code availability

Data generated in this study are available upon request from the Lead Contact.

EXPERIMENTAL MODEL AND SUBJECT DETAILS

Animal subjects

All experimental procedures and work utilizing mice were approved by The Scripps Research Institute's IACUC committee in compliance with guidelines set by the NIH. The mice were maintained under standard housing conditions in a pathogen-free facility under a 12/12 light/dark cycle where all mice had continuous access to food and water. The generation of *Gnao1*$^{flox/flox}$ and *RGS9*^{Cre} mouse lines have been previously described (Chamero et al., 2011; Dang et al., 2006). *Drd1a*^{Cre} (Drd1-Cre; EY262; stock# 017264-UCD) and *Drd2*^{Cre} (Drd2-Cre; ER43; Stock #: 017268-UCD) mouse lines were obtained from the Mutant Mouse Resource & Research Centers (MMRRC). Conditional knockout mice were generated by two rounds of crossing *Gnao1*$^{flox/flox}$ with *RGS9*^{Cre}, *Drd1a*^{Cre}, or *Drd2*^{Cre} to obtain homozygous *Gnao1*$^{flox/flox}$*:RGS9*^{Cre}, *Gnao1*$^{flox/flox}$*:Drd1a*^{Cre}, or *Gnao1*$^{flox/flox}$*:Drd2*^{Cre} and their wild-type control littermates (*Gnao1*$^{flox/flox}$). Mice were identified through standard PCR genotyping methods as previously described for each line. Behavioral studies exclusively utilized male mice. Biochemical studies utilized both male and female mice. All experiments were performed on mice between the age of 2-4 months.

Primary cultures

Striata from pups at age P0 from *Gnao1*$^{flox/flox}$, *Gnao1*$^{flox/flox}$*:Rgs9*^{Cre}, or *CAMPER* mice were dissected in ice-cold HBSS supplemented with 20% FBS, 4.2 mM NaHCO3, and 1 mM HEPES, as previously described (Muntean et al., 2018). Striata were washed in HBSS absent FBS and digested at 37C for 15 min in a pH 7.2 buffer containing (in mM): NaCl (137), KCl (5), Na2HPO4 (7), HEPES (25), and 0.3 mg/ml Papain (Worthington). Striata were then washed three times with each of the following solutions: HBSS/FBS, HBSS, growth media (Neurobasal-A supplemented with 2 mM GlutaMAX, 2% B27 Supplement, and 1% PenStrep). Tissue was dissociated with a standard P1000 pipette in the presence of DNase I (0.05 U/ul), cells were filtered through a 40 um cell strainer, and the plated on Poly-D-Lysine coated glass coverslips. Neuronal cultures were maintained at 37°C/5% CO_2 in a humidified incubator whereupon half of the growth media was replenished every three days. Transfection of $^{T}Epac^{VV}$ biosensor along with mutated *GNAO1* constructs was performed utilizing Lipofectamine 2000, as previously described (Masuho et al., 2018).

METHOD DETAILS

Behavioral studies

Rotarod

Rotarod performance was tested using a five-station rotarod treadmill (IITC Life Sciences, USA) with an acceleration from 8 to 20rpm. Rotarod testing consisted of six trials per day with 5 min between intertrial intervals, while daily testing consisted of four trials per day up to 6 consecutive days. Each trial ended when a mouse fell off the rod or completed one full revolution on the rod or reached 120 s and the time was scored as the latency to fall.

Grip strength tests

Grip strength was measured as the peak force using a grip strength meter (Ugo Basile Italy). Both forearms of mouse grasped the grid and the tail was pulled horizontally until the mouse released its hold entirely. Three separate readings were recorded for each mouse, with a corresponding 20 s between each trial.

Locomotion

Locomotor activity was performed in 40 × 40 × 35 chambers (Stoelting Co, Wood Dale, IL) and distance traveled was recorded using Anymaze video-tracking software. Mice were placed in the center of the chambers and distance traveled was measure for 60 mins and analyzed in 10 min bins.

Hindlimb clasping

As previously described (Guyenet et al., 2010), mice (males and females, approximately 3 months old) were held by base of tail, lifted in the air, and observed for 30 s. Animals were scored as followed: no clasping (0), clasping of 1 hindlimb part of the time (1), clasping of 1 hindlimb of the entire time (2), clasping of both hindlimbs part of the time (3), and clasping of both hindlimbs of the entire time (4). Animals were tested and scored once a day for 3 days.

Backward walking

Mice (males and females, approximately 3 months old) were placed into RotaRod apparatus (IITC Life Science Inc., Woodland Hills, CA USA) and made to walk backward. RotaRod was fitted to ensure that mice were not able to turn around and walk forward. Animals had walked backward from 1 s at 8.1 RPM and cut off time was 10 s at 9.15 RPM. Each mouse was tested once a day for 3 days. Latency to fall was recorded.

Ledge test

As previously described (Guyenet et al., 2010), mice (males and females, approximately 3 months old) were individually placed onto lip of house cage (Allentown Inc., Allentown, NJ USA) and observed for balancing and movement. Animals were scored as followed: balancing and walking well (0), good balance but teetering walk (1), teetering in balance and walk (2), teetering in balance but unable to walk (3), and falling off (4). Animals were tested and scored once a day for 3 days.

Vertical pole

As previously described (Matsuura et al., 1997), mice (males and females, approximately 3 months old) were placed nose facing up on a wooden pole (1 cm diameter) at 50 cm in height from bottom of mouse cage (Allentown Inc., Allentown NJ USA). In order to successfully complete this task with a score of 0, subjects had to turn around (nose facing down) and procced down the pole. Subjects that had turned around and climbed down the pole with some difficulty had received a score of 1. Subjects that had climbed down the pole without turning around had a score of 2. Animals which slid down the pole had a score of 3 and animals that fell off the pole had scored 4. Due to the nature of this study, there was no cut off time. Animals were tested and scored three times on the same day.

Horizontal pole

As previously described (Farr et al., 2006), mice (males and females, approximately 3 months old) were placed at 50 cm away from home cage (facing toward home cage) on a 1 cm diameter wooden pole. Mice were scored as followed: normal gait and balance to home cage (0), normal gait but unbalanced to home cage (1), both poor gait and balance to home cage (2), unable to complete task due to lack of movement (3), and falling off pole (4). Cut off time for sessions was 120 s. Animals were tested and scored three times on the same day.

CRISPR/Cas9 lentivirus

As previously described (Doyle et al., 2019; Muntean et al., 2018), three unique sgRNA sequences per gene were first designed with CHOPCHOP (https://chopchop.cbu.uib.no/) to target *Gnai1*, *Gnai2*, and *Gnai3* (Table S1). Custom oligos were obtained from Integrated DNA Technologies (Coralville, IA, USA) for *in vitro* phosphorylation by T4 polynucleotide kinase followed by an annealing reaction in a thermocycler and finally ligation into the pSECC vector (Addgene #60820) BsmBI site with T4 DNA Ligase. Three sgRNA constructs were made for each target gene, plasmids were purified from Stbl3 *E. coli*, and lentiviral particles were generated by Lipofectamine LTX-mediated transfection of 293FT cells with pSECC, pCMV-VSV-G (Addgene #8454), pMDLg/pRRE (Addgene #12251), and pRSV-Rev (Addgene #12253). The supernatant containing the lentiviral particles was collected at 48 hr post-transfection.

Confocal imaging

Coverslips containing neuronal cultures were transferred to a recording chamber for live imaging of the $^{T}Epac^{VV}$ biosensor (Klarenbeek et al., 2011) using a Leica TCS SP8 MP confocal microscope. Excitation of the mTurquoise FRET donor was achieved with a 442 nm diode laser which was paired with collection of bandpass emission filtration at 3.5 Hz simultaneously from 465-505 nm (mTurquoise FRET donor) and 525-600 nm (Venus FRET acceptor). Image stacks containing XYZ planes were acquired at 10 s intervals through a 25x objective lens. Quantification of fluorescence intensity was performed on neuronal cell bodies using ImageJ to calculate FRET from the inverse ratio of donor:acceptor. Absolute cAMP values were determined from interpolation of a cAMP standard curve in permeabilized CAMPER neurons (Muntean et al., 2018). Dopamine and adenosine were added in phasic puffs in the pH 7.2 recording buffer which consisted of (in mM): CaCl2 (1.3), MgCl2 (0.5), MgSO4 (0.4), KH2PO4 (0.4), NaHCO3 (4.2), NaCl (138), Na2HPO4 (0.3), D-Glucose (5.6), and HEPES (20). In dMSNs D1R stimulates and A1R inhibits cAMP whereas in iMSNs A2AR stimulates and D2R inhibits cAMP. Therefore, sign of cAMP response classified neurons as dMSN or iMSN without the need for additional reagents to isolate the cAMP signaling pathway.

Recombinant protein preparation

Recombinant Gαs and Gαi were purified as previously described (Lee et al., 1994). Gαo (human GαoA WT) was cloned into a modified pET28 vector with N-terminal $(Histidine)_8$ tag followed by PreScission Protease cleavage site (LEVLFQGP) and purified from the BL21(DE3) *E. coli* strain. Briefly, the *E. coli* cells were grown at 37°C to an OD_{600} = 0.6 and induced by 0.1mM isopropyl-thiogalactoside (IPTG) for 16-18 h at 18°C. The cells were harvested, resuspended in buffer A (50 mM Tris (pH 8), 500 mM NaCl, 5 mM β-ME, 5 mM $MgCl_2$, 10 mM imidazole, 10 μM GDP) having complete protease inhibitor tablets (Roche), disrupted by sonication and clarified by centrifugation at 32,000 rpm for 45 min. The cell lysate was loaded onto a pre-equilibrated HisTALON Superflow Cartridge (Clontech Laboratories, Inc.) with buffer A and eluted over a 250 mM imidazole gradient. Fractions containing Gαo were pooled, diluted with buffer A without NaCl to obtain final NaCl concentration to 40 mM. PreScission Protease was added to the pooled fractions to remove histidine tag and incubated overnight at 4°C. Histidine tag free Gαo was collected as flow through (FT) upon loading sample on HisTALON Superflow Cartridge. FT was further loaded onto a Mono Q 4.6/100 PE column (GE Healthcare) and eluted over a 500 mM NaCl gradient. The eluted protein was further purified using Hiload 26/60 Superdex 75 column (GE Healthcare) which was pre-equilibrated with buffer B (20 mM HEPES (pH 8), 200 mM NaCl, 2 mM DTT, 5 mM $MgCl_2$,

10 μM GDP). The purity of the protein was analyzed by SDS-PAGE, pooled, concentrated to 20 mg/ml and stored at −80°C. Gα proteins were activated by incubating with 20 μM GTPγS in a buffer composed of 20 mM Tris-HCl pH 7.8, 10 mM MgCl2, 1 mM EDTA, 1 mM dithiothreitol for 30 min (Gαs and Gαo) or 2 hr (Gαi) at 30°C. Zeba spin desalting column (Life Technologies, Carlsbad, CA) was then used to remove unbound GTPγS. Recombinant complexes of Gβ1 with His-tagged Gγ2 were expressed in Sf9/baculovirus system and purified as described (Xie et al., 2012). His-PDEγ(63-87) was purified as described (Arshavsky et al., 1994) for pulldown assay with recombinant Gαi/o. Briefly, recombinant Gαi/o (2 μM) and PDEγ (2 μM) were incubated with Ni-NTA beads for 30 min at 30°C at 300 rpm in a buffer containing 20 mM HEPES pH 8, 300 mM NaCl, 20 mM Imidazole, 5 mM MgCl2, 1 mM dithiothreitol, and 1% Triton X-100. The beads were then washed 3 times with 1 mL buffer, proteins eluted with SDS buffer, and visualized on a Coomassie stained SDS gel.

Adenylyl cyclase assay

As previously described (Orlandi et al., 2019; Xie et al., 2012), striatal membranes were isolated from flash frozen (liquid nitrogen) 2 mm tissue punches (dorsal striatum) by homogenization in 20 mM HEPES pH 8.0, 1 mM EDTA, 150 mM NaCl, 2 mM MgCl2, 1 mM dithiothreitol, and cOmplete protease inhibitor (Roche, Indianapolis, IN) followed by centrifugation at 2000 × g to clear debris. The resulting supernatant was then ultracentrifuged in a Beckman SW28.1 rotor at 25,000 rpm for 35 min over a 23/43% sucrose emulsion. The plasma membrane fraction was collected at the sucrose interface and protein concentration was determined (Pierce 660 nm Protein Assay Reagent, Thermo Fisher Scientific, Waltham, MA). In assays of adenylyl cyclase inhibition, 2 μg of WT striatal membrane per reaction was stimulated by forskolin (300 μM) simultaneously with Gαi- or Gαo-GTPγS for 10 min at 30°C. In assays of Gβγ effect during adenylyl cyclase inhibition, 2 μg of WT striatal membrane per reaction were pre-incubated with 1 μM Gβ1γ2 for 30 min at 4°C prior to stimulation with forskolin (300 μM) and Gαi-GTPγS for 10 min at 30°C. In assays of endogenous Gαo role, 2 μg of *Gnao1*$^{flox/flox}$ and *Gnao1*$^{flox/flox}$*:RGS9*^{Cre} striatal membranes per reaction were stimulated by forskolin for 10 min at 30°C. In assays of Gβγ inhibition, 2 μg of striatal membrane per reaction were pre-incubated with 100 μM Grk2i-peptide (Tocris) for 30 min at 4°C prior to stimulation with Gαs-GTPγS for 10 min at 30°C. In assays of agonist-induced cAMP generation, 2 μg of striatal membrane per reaction were pre-incubated with 10 μM SKF81297 or 10 μM CGS21680 (Tocris) for 10 min at 30°C. All reactions were quenched by an equivalent volume of 0.2 M HCl. As previously described, the assay buffer for reactions consisted of 50 mM HEPES (pH 8.0), 0.6 mM EDTA (pH 7.0), 100 μg/ml bovine serum albumin, 3 mM phosphoenolpyruvate potassium, 10 μg/ml pyruvate kinase, 5 mM $MgCl_2$, 100 μM ATP, 10 μM GTP, and 100 μM IBMX (Dessauer, 2002).

cAMP measurements

For assessment of total brain cAMP level, dorsal striatal tissue punches (2 mm) were flash frozen in liquid nitrogen followed by homogenization in 0.1M HCl. Levels of cAMP were then determined (tissue punches and adenylyl cyclase assays) by diluting samples (between 1:20 and 1:50) in 0.1 M HCl followed by quantification with a competitive cAMP enzyme immunoassay following the acetylated protocol described in the manufacturer's guidelines (Direct cAMP ELISA kit, ENZO Life Sciences, Farmingdale, NY).

Immunoprecipitation

Freshly dissected striata (~20 mg) from *Gnao1*$^{flox/flox}$ and *Gnao1*$^{flox/flox}$*:Rgs9*^{Cre} were homogenized in 1 mL lysis buffer (PBS supplemented with 150 mM NaCl, Roche cOmplete protease inhibitor, Sigma Phosphatase Inhibitor Cocktails 2 and 3, and 0.5% non-ionic detergent C12E9), sonicated for 15 s, and slowly rotated for 15 min at 4°C followed by centrifugation at 16,000 x g for 15 min at 4°C. The supernatant of each sample was diluted to the same concentration and 400 μg was incubated with 3 μg anti-AC5 antibody (Xie et al., 2015) and 50 μL Dynabeads Protein G (ThermoFisher) for 1 hr while rotating at 4°C. The beads were then washed three times with 1 mL of lysis buffer followed by elution with urea sample buffer, incubation for 15 min at 42°C, and Western analysis.

Western blotting

For brain samples, tissue punches of the striatum were homogenized in ice-cold buffer (137 mM NaCl, 20 mM Tris (pH 8.0), 1% NP-40, 10% glycerol and 0.1% sodium dodecyl sulfate) with the addition of protease and phosphatase inhibitors (Roche, Rockford, IL) and then sonicated. Protein concentration of tissue lysates was determined by Pierce 660 nm Protein Assay Reagent (Thermo Fisher, Waltham, MA) and samples were diluted to the same concentration and denatured in SDS buffer. For cultured cells, each sample of about 5 × 10^6 cells were lysed in 500 ul of sample buffer (125 mM Tris-HCl, pH 6.8, 4 M urea, 4% SDS, 10% 2-mercaptoethanol, 20% glycerol, bromophenol blue (0.16 mg/ml)). Western blotting analysis of proteins was performed after samples were resolved by SDS–polyacrylamide gel electrophoresis and transferred onto PVDF membranes. Blots were blocked with 5% skim milk in PBS containing 0.1% Tween 20 (PBST) for 30-90 min at room temperature (22–26°C). To detect the proteins of interest membranes were incubated with the following primary antibodies: AC5 (1:3000) (Xie et al., 2015), Gαo (Cell signaling, cs-3975, 1:1000), Gαolf (Corvol et al., 2001), Gβ1 (Lee et al., 2004), Gβ2 (C-16) (Santa Cruz, sc-380), GAPDH (Millipore AB2302, 1:25,000), pAkt473 (Cell signaling, cs-4060, 1:1000), Akt (Cell signaling, cs-2920, 1:1000), pERK (Cell signaling, cs-9101, 1:1000), ERK Cell signaling, cs-4695, 1:1000), GSK-3 (Cell signaling, cs-5676, 1:1000) and pGSK-3 (Cell signaling, cs-9331, 1:1000). Blots were washed in PBST and incubated with secondary antibodies conjugated with horseradish peroxidase in PBST containing 1% skimmed milk. All protein signals were visualized using Kwik Quant Imager (Kindle Biosciences) and band intensities were determined using NIH ImageJ software.

cDNA constructs

Dopamine D2 receptors (D2R) (NM_000795) tagged with myc and SmBiT at the C terminus of D2R (D2R-myc-SmBiT), GαoA (NM_020988) and mutant GαoA in pcDNA3.1(+) were synthesized by GenScript. Flag-tagged D2R (Flag-D2R) (NM_000795) containing the hemagglutinin signal sequence (KTIIALSYIFCLVFA) at the N terminus was a gift from Dr. Abraham Kovoor (Celver et al., 2012). Venus 156-239-Gβ1 (amino acids 156-239 of Venus fused to a GGSGGG linker at the N terminus of Gβ1 without the first methionine (NM_002074)) and Venus 1-155-Gγ2 (amino acids 1-155 of Venus fused to a GGSGGG linker at the N terminus of Gγ2 (NM_053064)) were gifts from Dr. Nevin A. Lambert (Hollins et al., 2009). The masGRK3ct-Nluc-HA constructs were constructed by introducing HA tag at the C terminus of masGRK3ct-Nluc-HA reported previously (Masuho et al., 2015b). Nluc was inserted between residues 91 and 92 of GαoA (NM_020988) with SGGGGSGGGGS linker at the N terminus and C terminus of the Nluc to make GαoA-Nluc. D2R-myc-SmBiT was generated by introducing myc epitope tag, VSQGSSGGGGSGGGGSSG linger, and SmBiT tag at the C-terminal end of D2R. GαoA-Nluc and D2R-myc-SmBiT were inserted into the mammalian expression vector pcDNA3.1(+). pcDNA3.1(+) was purchased from Thermo Fisher Scientific. GenBank accession number for each sequence is given in brackets.

Cell culture and transfection

HEK293T/17 cells were grown in DMEM supplemented with 10% FBS, minimum Eagle's medium non-essential amino acids, 1mM sodium pyruvate, and antibiotics (100 units/ml penicillin and 100 μg/ml streptomycin) at 37°C in a humidified incubator containing 5% CO_2. For transfection, cells were seeded into 6-cm dishes at a density of 4 × 10^6 cells/dish. After 2 h, expression constructs (total 10 μg/dish) were transfected into the cells using PLUS (10 μl/dish) and Lipofectamine LTX (12 μl/dish) reagents. For BRET assay, Flag-D2R (1), GαoA (2), Venus 156-239-Gβ1 (1), Venus 1-155-Gγ2 (1), and masGRK3ct-Nluc-HA (1) were transfected. For NanoBiT assay D2R-myc-SmBiT (1), GαoA (2), LgBiT-Gβ1 (1), and Gγ2 (1), were transfected. For Gα and Gβγ dissociation assay, Flag-D2R (1), GαoA-Nluc (0.1), Venus 156-239-Gβ1 (1), and Venus 1-155-Gγ2 (1) were transfected. The number in brackets indicates the ratio of transfected DNA (ratio 1 = 0.42 μg). An empty vector (pcDNA3.1(+)) was used to normalize the amount of transfected DNA.

BRET assay

Cellular measurements of BRET between Venus-Gβ1γ2 and masGRK3ct-Nluc-HA were performed to examine trimer formation, agonist-induced G protein activation, and dominant-negative activity of Gαo mutants in living cells (described in detail in Masuho et al., 2015a, 2015b). Sixteen to twenty-four hr post-transfection, HEK293T/17 cells were washed once with BRET buffer (Dulbecco's Phosphate-Buffered Saline (PBS) containing 0.5mM $MgCl_2$ and 0.1% glucose) and detached by gentle pipetting over the monolayer. Cells were harvested with centrifugation at 500 g for 5 min and resuspended in BRET buffer. Approximately 50,000 to 100,000 cells per well were distributed in 96-well flatbottomed white microplates (Greiner Bio-One). The substrate for Nano luciferase (Nluc), furimazine, were purchased from Promega and used according to the manufacturer's instruction. BRET measurements were made using a microplate reader (POLARstar Omega; BMG Labtech) equipped with two emission photomultiplier tubes, allowing detection of two emissions simultaneously with a highest possible resolution of 20 ms per data point. All measurements were performed at room temperature. The BRET signal is determined by calculating the ratio of the light emitted by the Venus-Gβ1γ2 (535 nm with a 30 nm band path width) over the light emitted by the masGRK3ct-Nluc-HA (475 nm with a 30 nm band path width). The average baseline value (basal BRET ratio) recorded prior to agonist stimulation was subtracted from the experimental BRET signal values.

NanoBiT assay

Interaction of D2R-myc-SmBiT with G protein consisted of exogenously transfected GαoA (wild-type or mutant), LgBiT-Gβ1, and Gγ2 was examined with NanoBiT assay. Transfected cells were harvested and distributed in 96-well plates as explained above. Furimazine was added and incubated for 1 min to stabilize the brightness of luminescence before dopamine application, and then luminescence was measured using a POLARstar Omega at room temperature.

Adeno-associated viruses (AAV) and stereotaxic injections

Mice were anesthetized with isoflurane and the head was fixed on a Kopf stereotaxic apparatus. The animals were kept warm (~37°C) for the whole duration of the surgery via a heating pad connected to a DC temperature controller provided with a feedback system (FHC Inc.). An eye lubricant was applied to prevent corneal drying during the surgery. Adeno-associated virus (AAV) encoding the fluorescent protein EYFP (AAV5-EF1a-DIO-EYFP) was obtained from the Vector Core at the University of North Carolina at Chapel Hill (UNC Vector Core, USA). AAV encoding *GNAO1* variants (AAV9-Syn-DIO-Gαo-IRES-mCherry) were obtained from VectorBuilder (Chicago, IL). Viral injections were targeted to the dorsal striatum (AP +0.7, ML ± 1.5 relative to bregma, DV −1.7 relative to dura). The injection volume (300 nl) and flow rate (50 nl/min) were controlled with an injection pump (Cemyx Nanojet, USA). The needle was left in place for 5 min after the injection and then slowly withdrawn. Mice were allowed to recover for at least 15 days before electrophysiological experiments.

Slice electrophysiology

Mice aged 8-12 weeks old were anesthetized with isoflurane and decapitated. The brain was quickly removed and rested for 30 s in ice-cold oxygenated NMDG cutting solution containing (in mM): 93 NMDG, 2.5 KCl, 1.2 NaH_2PO_4, 30 $NaHCO_3$, 20 HEPES, 25 glucose, 2 thiourea, 5 Na-ascorbate, 3 Na-pyruvate, 0.5 $CaCl_2$·, 10 $MgCl_2$, (adjusted to 7.2–7.4 pH with HCl). Coronal slices

(300 μm thick) containing the striatum were cut on a vibratome (VT1200S, Leica) and incubated for 30 min at 34°C in oxygenated ACSF containing the following (in mM): 126 NaCl, 2.5 KCl, 2 CaCl2, 2 MgCl2, 18 NaHCO3, 1.2 NaH2PO4, 10 glucose, then allowed to recover for at least 1 hr at room temperature before recording. Whole cell recordings were obtained from MSNs in the dorsal striatum using a Scientifica SliceScope system. Pipets (4-6 MΩ) were pulled by P-1000 (Sutter Instruments, CA) and filled with an intracellular solution containing the following (in mM): 119 K-MeSO4, 12 KCl, 1 MgCl2, 0.1 CaCl2, 10 HEPES, 1 EGTA, 0.4 Na-GTP, 2 Mg-ATP, (280–300 mOsm, pH 7.3 adjusted with KOH). Recordings were performed in a chamber perfused with ACSF at a rate of 2 ml/min and maintained at 32°C. Somatic EYFP expression was verified in cell-attach mode to confirm cell identity before breaking into whole-cell mode. Current-clamp recordings were performed to quantify intrinsic membrane properties from fluorescent MSNs from *Drd1a*^{Cre} and *Drd2*^{Cre} which were used as controls and compared with MSNs from *Gnao1*$^{flox/flox}$:*Drd1a*^{Cre} and *Gnao1*$^{flox/flox}$:*Drd2*^{Cre}. Spikes were evoked using current step injections (500-ms duration at 0.2 Hz, −200 to +500 pA range with increasing 20 pA steps). Rheobase current was defined as the first current step capable of eliciting one action potential. Input resistance was measured with a 120 pA hyperpolarizing step from the resting membrane potential. For voltage-clamp experiments, pipettes (3-5 MΩ) were filled with Cs+ internal solution containing the following (in mM): 120 CsMeSO3, 15 CsCl, 8 NaCl, 10 TEA-Cl, 10 HEPES, 2-5 QX-314, 0.2 EGTA, 2 Mg-ATP, 0.3 Na-GTP, pH 7.3 adjusted with CsOH. To record miniature excitatory post-synaptic currents (mEPSCs) MSNs were clamped at −70 mV and TTX (1 μM) and picrotoxin (100 μM) were added to the recording solution. Evoked EPSCs were recorded using a bipolar stimulating electrode located ∼200 μm away from the recorded soma. AMPA/NMDA ratios of evoked EPSC were obtained by measuring AMPA-EPSC at −70 mV/NMDA-EPSCs at +40 mV. NMDAR-mediated EPSCs were measured 60 ms after the stimulus onset. Mean EPSCs were calculated from an average of 15 sweeps obtained at 0.05 Hz. Acquisition was done using Clampex 10.5, MultiClamp 700B amplifier and Digidata 1440A (Molecular Devices, CA). Data were analyzed with Clampfit 10.5.

Fast-Scan Cyclic Voltammetry (FSCV)

Custom carbon fiber electrodes were made in-house and inserted into a glass pipette (50-100 μm in length, 7 μm diameter, T-795, GoodFellow Corp. Coraopolis, PA). Electrodes were cleaned with bleach to improve sensitivity and pre-calibrated with dopamine. Electrodes were inserted 50-100 μm below the surface of acute striatal slices. To distinguish dopamine from other catecholamines (Rice et al., 1997), extracellular dopamine levels were monitored as current generated by application of a triangular waveform (−0.4 to +1.0 to −0.4 V versus Ag/AgCl at 200 V/sec scan speed) every 100 msec (10 Hz). The peak of oxidation current at +400mV was measured after background current subtraction. All data were acquired using a MultiClamp 700B amplifier (Molecular Devices, Sunnyvale, CA) with 4kHz high-pass filter and digitized in Digidata1550B (Molecular Devices) at 10kHz. Electrical stimulation was provided by a 50 μm diameter twisted tungsten wire stimulating electrode (A-M Systems, Sequim, WA) placed in close proximity to the carbon fiber electrode. Electrical stimulation was also applied at 20 Hz for 1sec (10V, 200 μs pulse duration) delivered from an isolated pulse stimulator (Model 2100, A-M systems).

In situ hybridization

As similarly described (Sutton et al., 2016), The ViewRNA 2-plex *In Situ* Hybridization Assay kit was utilized to evaluate mRNA expression with probes selective for Drd1 (NM_010076.3; Assay ID VB6-12478), Drd2 (NM_010077.2; Assay ID VB6-16550), and Gnao1 exon5_6 (NM_010308; Assay ID VPMFWXD). DAPI mounting media was used to visualize the nucleus. Confocal images of the dorsal striatum were acquired through a 10x objective lens on a Leica TCS SP8 MP confocal microscope. Images were acquired from *Gnao1*$^{flox/flox}$ (n = 4 mice), *Gnao1*$^{flox/flox}$ (n = 2 mice):*RGS9*^{Crex} (n = 2 mice), *Gnao1*$^{flox/flox}$:*Drd1a*^{Cre} (n = 2 mice), and *Gnao1*$^{flox/flox}$:*Drd2*$^{Cr\ e}$ (n = 2 mice) using non-saturating fluorescence intensity settings.

QUANTIFICATION AND STATISTICAL ANALYSIS

Statistical analysis was performed using GraphPad Prism 8. Unless otherwise indicated, all data are represented as mean ± SEM. Student t test, nonparametric tests, one-way ANOVA, and two-way ANOVA followed by indicated posttest were utilized as well as number of biological replicates are described in appropriate figure legends for each experimental comparison. F-test parameters for dose-response experiments are reported in Table S2. The use of asterisks indicate statistical significance (* = $p < 0.05$, ** = $p < 0.01$, *** = $p < 0.001$, **** = $p < 0.0001$).